EURASIP Journal on Wireless Communications and Networking

RESEARCH Open Access

Joint beamforming and power splitting design for MISO downlink communication with SWIPT: a comparison between cell-free massive MIMO and small-cell deployments

Jain-Shing Liu[1*], Chun-Hung Richard Lin[2†] and Wan-Ling Chang[3†]

†Chun-Hung Richard Lin and Wan-Ling Chang contributed equally to this work.

*Correspondence: chhliu@pu.edu.tw

[1] Computer Science and Information Engineering, Providence University, 200, Sec. 7, Taiwan Boulevard, Taichung 43301, Taiwan
[2] Computer Science and Engineering, National Sun Yat-sen University, No. 70, Lienhai Rd., Kaohsiung 80424, Taiwan
[3] Insurance, Chaoyang University of Technology, 168, Jifeng E. Rd., Taichung 413310, Taiwan

Abstract

Simultaneous wireless information and power transfer (SWIPT) has been advocated as a highly promising technology for enhancing the capabilities of 5G and 6G devices. However, the challenge of dealing with large propagation path loss poses a significant hurdle. To address this issue, massive multiple-input multiple-output (MIMO) is employed to enhance the efficiency of SWIPT in cellular-based networks with multiple small cells, and especially increase the energy for cell-edge users. In addition, by leveraging a large set of spatially distributed base stations to collaboratively serve SWIPT-enabled user equipment, the cell-free massive MIMO has the potential to provide even better performance than the conventional small-cell systems. In this work, we extend the investigation to include the application of SWIPT technology with alternating current (AC) logic in the cell-free networks and the small-cell networks and propose joint beamforming and power splitting optimization frameworks to maximize the system sum-rate, subject to the constraints on harvested energy, AC logic energy supply, and total transmit power. The optimization problem is shown to be non-convex, posing a significant challenge. To address this challenge, we resort to a two-stage decomposition approach. Specifically, we first introduce quadratic transform-based fractional programming (FP) algorithms to iteratively solve the non-convex optimization problems in the first stage, achieving near-optimal solutions with low time complexities. To further reduce the complexities, we also incorporate conventional schemes such as zero forcing, maximum ratio transmission, and signal-to-leakage-and-noise ratio for the design of beamforming vectors. Second, to determine the optimal power splitting ratio within the framework, we develop a one-dimensional (1-D) search algorithm to tackle the single variable optimization problem reduced in the second stage. These algorithms are then evaluated in the context of cell-free MIMO and small-cell networks with numerical experiments. The results show that the FP-based algorithms can consistently outperform those utilizing the conventional beamforming schemes, and the solutions of this work can achieve up to fivefold improvement in the system sum-rate than the small-cell counterpart while providing different but comparable performance trends in energy harvesting (EH).

Keywords: Joint design, Beamforming, Power splitting, Simultaneous wireless information and power transfer, Cell-free versus small-cell

1 Introduction

Conventionally, cellular networks are constrained by inter-cell interference, wherein a user close to cell boundary would particularly suffer from strong interferences from neighbouring base stations (BSs). To alleviate this problem, the technique of network multiple-input multiple-output (MIMO), which is also referred to as distributed MIMO or coordinated multi-point transmission (CoMP), is proposed by means of a coherent cooperation among BSs to reduce such interferences [1, 2]. For this aim, BSs in network MIMO require advanced backhaul links to support the signal transmission in the downlink (DL) and the signal detection in the uplink (UL). In addition, it requires a central processing unit (CPU) to collect the precoded signals and channel state information (CSI) among BSs. By bearing these costs, the cooperation can yield significant improvements on spectrum efficiency (SE) and coverage probability [3, 4], inspiring many related studies [5–12].

As a variant of the above, cell-free massive MIMO has been introduced and gained much interest recently, in which a large number of BSs equipped with several antennas is adopted to serve a relatively smaller number of user equipment (UEs) that share the same time-frequency resources. Herein, each UE would be surrounded by a considerable number of BSs, thereby experiencing a high degree of macro-diversity and low path losses. This implies a uniformly good level of quality-of-service (QoS) to be perceived by a UE despite its particular location in the network. Given the special merit, [13] has demonstrated that cell-free massive MIMO would pave a scalable way to implement CoMP and [14] exhibited that it has significantly superior performance than conventional small-cell networks, where each user is only served by a single BS.

Despite the differences between cell-free MIMO and small-cell, energy consumption is always an issue in networking, and energy harvesting (EH) would be one of the most important solutions to address this issue, especially for the massive amount of lower-powered wireless devices deployed in the Internet of Things (IoT) [15, 16]. For efficient EH, simultaneous wireless information and power transfer (SWIPT) has been widely adopted as a special case of the wireless power transfer (WPT) system. As the name implies, SWIPT allows for the simultaneous transfer of both information and power, and it is beneficial for ensuring an acceptable level of EH without the need for costly infrastructure upgrades [17, 18].

In conventional small-cell networks, SWIPT is usually studied by means of co-located massive MIMO [19–24]. For example, [19] formulated achievable data rate and EH expressions for the SWIP-enabled massive MIMO systems over Rician fading channels. Similarly, [20] proposed to jointly decide transmit power and time-slot duration in order to optimize energy efficiency (EE) subject to its QoS constraints in the SWIPT-enabled system with energy beamforming. In addition, joint optimization of beamforming and power splitting has also received significant attention in SWIPT-enabled networks. Specifically, the joint optimization problem of satisfying both signal-to-inference-and-noise ratio (SINR) and harvested power constraints at each user with minimum transmission

power has been addressed in [21], for instance. In that work, a feasible point pursuit-successive convex approximation (FPP–SCA) method was introduced to address the minimization problem for the total power of beamforming vectors (BVs). Moreover, for simultaneously optimizing data rates and harvested powers in such networks, the authors in [22] proposed a majorization–minimization (MM) approach, which could outperform the classical block-diagonalization (BD) strategy. Additionally, other optimization objectives, such as maximizing the minimum (or max–min) throughput and energy, have also been proposed [23, 24].

Unlike the aforementioned progress on SWIPT, early research on cell-free massive MIMO networks primarily focused on developments without SWIPT [25–28]. For example, in [25], an optimization problem was presented to jointly determine non-orthogonal pilot sequences and base stations (BSs), aiming to maximize the achievable UL and DL rates through the proposed transmit power control. In [26], a distributed conjugate beamforming method was proposed for the multi-group multicast cell-free massive MIMO network. Similarly, a minimum mean square error (MMSE)-based precoding was introduced in [27] for cell-free massive MIMO systems. Furthermore, a joint optimization model for DL beamforming and power control was proposed in [28], and a joint beamforming and power optimization framework for massive MIMO systems can be found in [29].

After the initial works, cell-free massive MIMO has made further progress with the integration of WPT. Particularly, in the scenario where UEs can utilize the energy harvested in DL to transmit UL pilot and information signal to BSs, the authors in [30, 31] aimed to maximize the minimum SE of UEs while considering the transmission power constraints of both BSs and UEs. In addition, a wirelessly powered IoT system based on the cell-free massive MIMO technology has also been proposed in [32], where the UL and DL power control coefficients are jointly optimized to minimize the total transmit energy consumption while satisfying the target SINRs. Then, a long-term scheduling and power control approach to maximize the minimum time-average data rate among all sensors in WPT-aided cell-free IoT networks was further studied in [33]. Additionally, the expressions for the average DL data rate for EH users based on stochastic geometry were derived in [34], including the coexistence of cell-free massive MIMO and SWIPT.

Despite the different types of networks as mentioned, most related works on SWIPT considered a linear EH model, which rectifies the received radio frequency (RF) signals into required direct current (DC) power through RF-EH circuits. However, the process of rectification can result in losses, leading to a decrease in EE. More recently, based on power splitting, a receiver architecture was proposed in [35], allowing computing circuits powered directly with alternating current (AC) voltages rather than direct current (DC) for the SWIPT receiver. Given the innovation, this work, however, studied only a simple point-to-point link configuration as an example. Here, we extend the information decoding and energy harvesting (ID-EH) receiver architecture to consider the multiple input single output (MISO) interference channel (IC) in the small-cell networks,[1] and the cell-free massive MIMO networks. Building on the

[1] In the conventional small-cell scenario, each UE is served only by its own BS for transmitting information. However, with the aid of SWIPT, each UE can harvest energy from not only its serving BS but also other BSs in the network while still receiving its own information.

Table 1 Summary of the related works

Classification		References
Environment	Small-cell	[14, 19–29, 37], this work
	Cell-free	[14, 25–34, 36], this work
Energy	SWIPT	[17–24, 34, 35], this work
	Non-SWIPT	[1–16, 25–33, 36, 37]
Comparison	Comparative	[14], this work
	Non-comparative	[1–13, 15–37]

extended architecture, we propose a joint beamforming and power splitting optimization framework to maximize the sum-rate while meeting energy constraints, AC logic energy supply, and total transmit power for both types of networks.

The framework, however, has intractable optimization forms mainly due to the AC computing involved. To tackle the challenge, we introduce a quadratic transform-based fractional programming (FP) model to address the non-convex optimization problem on beamforming for each type of network and provide near-optimal solutions while using a one-dimensional search algorithm to determine power splitting ratios (PSRs). To further reduce the computational complexities, we propose alternative solutions based on conventional beamforming schemes such as zero forcing (ZF), maximum ratio transmission (MRT), and signal-to-leakage-and-noise ratio (SLNR) to solve the beamforming design problem, while leaving the one-dimensional search algorithm in the above to determine PSRs. Especially unlike the previous works [14, 36, 37] that consider the conventional beamforming schemes adopted in non-SWIPT wireless networks for cell-free [36], small-cell [37], or both [14], we focus on developing the FP-based algorithms tailored for the SWIPT-enabled networks, along with their variants based on the conventional beamforming schemes. Furthermore, we conduct a comparative analysis of these FP algorithms and their variants, spanning both types of networks, similar to the approach in [14], which also considers both of the network scenarios. Beyond the perspective of scenarios, our study also provides insights into EH aspects, which were not addressed in the previous works. More specially, we categorized the reviewed literature based on their environment (small-cell or cell-free), energy harvesting (SWIPT or non-SWIPT), and whether they employed a comparative study (comparative or non-comparative). This categorization is now presented in Table 1. While the table reveals a considerable number of works across the considered spectrum, only a limited number of comparative studies exist apart from our work, such as that in [14]. In that work ([14]), it, however, does not consider SWIPT. In contrast, our comparative work not only encompasses beamforming methods across the spectrum but also integrates the AC-relevant SWIPT technique to tackle the non-convex optimization problem for both BV and PSR in these environments. In summary, the key characteristics and contributions of our work are as follows:

- We improve EE by extending the concept of AC computing to power the computation circuits with AC power in both cell-free MIMO networks and small-cell

networks. The nonlinear extension is then utilized by the proposed algorithms to manage the trade-off between ID and EH under varying transmission conditions.

- We formulate a joint optimization problem on designing DL BVs and determining PSRs for each type of network so that the sum-rate can be maximized subject to harvested energy, AC logic energy supply, and total transmit power constraints.
- For the non-convex optimization problems resulted, we propose FP-based algorithms to provide near-optimal solutions with low-computational complexity. To further reduce the complexity, we introduce alternative solutions based on conventional schemes such as ZF, MRT, and SLNR to solve the beamforming problem while leaving the one-dimensional search algorithm in above to solve the PSR problem.
- We quantitatively compare the performance of cell-free massive MIMO with that of small-cell in the SWIPT-enabled networks, showing that the solutions for cell-free can achieve up to a fivefold improvement in the system sum-rate when compared to small-cell, while providing different but comparable performance trends in EH for both types of networks, which is not explicitly shown in previous works.

The rest of this paper is structured as follows: In Sect. 2, we present the system and channel models for cell-free massive MIMO networks considered in this work. Based on these models, we then formulate the joint design optimization problem for cell-free networks. To address this problem, we propose a quadratic transform-based fractional programming algorithm in Sect. 3, followed by a sequential beamforming and power splitting algorithm in Sect. 4. Next, we introduce the system model and problem formulation for small-cell networks in Sect. 5. In this context, a corresponding fractional programming algorithm is presented to optimize the problem in Sect. 6, along with a sequential algorithm in Sect. 7. Numerical experiments are then conducted in Sect. 8 to compare the proposed algorithms. Finally, conclusions are drawn in Sect. 9.

Notations In this work, we follow the writing convention where boldface lowercase and uppercase symbols represent vectors and matrices, respectively. The superscripts $(\cdot)^{-1}$, $(\cdot)^{+}$, $(\cdot)^{\dagger}$, $(\cdot)^{\star}$, and $(\cdot)^{T}$ denote the matrix inverse, Moore–Penrose pseudo-inverse, conjugate transpose, conjugate, and transpose, respectively. The absolute value operator is denoted by $|\cdot|$, and the Euclidean norm is shown by $||\cdot||$. Additionally, the operation $\mathrm{Re}\,(\cdot)$ represents the real part of a complex number, $\mathbf{I}_M$ stands for an $M \times M$ identity matrix, and $\#\{K\}$ signifies the cardinality of the set K.

2 Methods

In this section, we introduce the system and channel models and formulate the joint design optimization problem for cell-free massive MIMO networks. Then, due to the extensive content of the corresponding methods, we organize them into Sects. 3 and 4 and for detailed exposition. Afterwards, we transition to addressing the system model and problem formulation for small-cell networks in Sect. 5, along with a detailed discussion of the methods specific to the small-cell scenario in Sects. 6 and 7.

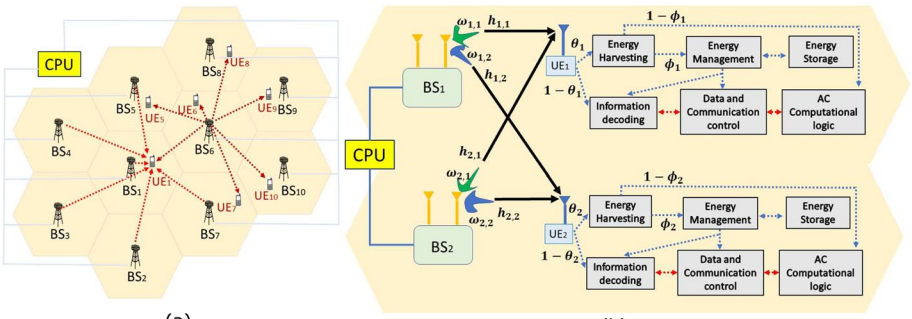

Fig. 1 Cell-free mass MIMO network: **a** system model, and **b** SWIPT architecture with integrate ID and EH (a two-BSs example)

2.1 System model

As shown in Fig. 1a, a cell-free massive MIMO network is considered to consist of a set of BSs, $\mathbb{B} = \{\mathrm{BS}_1, \mathrm{BS}_2, \ldots, \mathrm{BS}_{N_b}\}$, where $N_b = \#\{\mathbb{B}\}$ is the number of BSs in $\mathbb{B}$. In this network, an ideal backhaul link is assumed to connect all BSs with a central processing unit (CPU). These BSs serve a set of UEs, $\mathbb{U} = \{\mathrm{UE}_1, \mathrm{UE}_2, \ldots, \mathrm{UE}_{N_u}\}$, where $N_u = \#\{\mathbb{U}\}$ is the number of UEs in $\mathbb{U}$. In addition, each BS can employ $M_{\mathrm{BS}} > 1$ antennas, while each UE would use only a single antenna for operations. Given that, a UE-BS association is typically performed to enable each UE to be served by a subset of BSs in the network, including a set of all BSs in the conventional sense. Further, the set of BSs serving UE j is denoted by $\mathbb{B}_j = \{\mathrm{BS}_{j_1}, \mathrm{BS}_{j_2}, \ldots, \mathrm{BS}_{j_{n_b}}\}$. Similarly, BS i can serve a subset of UEs, denoted by $\mathbb{U}_i = \{\mathrm{UE}_{i_1}, \mathrm{UE}_{i_2}, \ldots, \mathrm{UE}_{i_{n_u}}\}$. For example, $\mathbb{B}_1 = \{\mathrm{BS}_1, \mathrm{BS}_2, \mathrm{BS}_3, \mathrm{BS}_4, \mathrm{BSBS}_5, \mathrm{BS}_6, \mathrm{BS}_7\}$ and $\mathbb{U}_6 = \{\mathrm{UE}_1, \mathrm{UE}_5, \mathrm{UE}_6, \mathrm{UE}_7, \mathrm{UE}_8, \mathrm{UE}_9, \mathrm{UE}_{10}\}$ as shown in Fig. 1a.

2.2 Channel model

Next, we consider a flat-and-block fading channel model, which is widely used for mmWave networks in 5 G and 6 G [38–40] to conduct the cell-free network. The model has also been investigated for massive MIMO networks in which the channel is almost flat within a resource block [41] and could be efficiently estimated [38, 40, 41]. Furthermore, the model allows incorporating specific space-time coding schemes into massive MIMO. For example, Bell Labs layered space-time (BLAST) coding, which achieves high spectral efficiency by using multiple antennas to transmit multiple data streams simultaneously, along with dirty paper coding, has been adopted in [42] to conduct a hybrid beamforming scheme for massive MIMO under the flat-fading channel model.

Specifically, this model involves several key notations. First, the fading coefficient including the path-loss and shadowing between BS i and UE j in time t is denoted by $\beta_{i,j}[t]$, while the complex path gain in time t is represented by $\alpha^p_{i,j}[t]$. Then, the array response vector corresponding to the angle of departure $\phi^p_{i,j}[t]$ is denoted by $a(\phi^p_{i,j})[t]$, and the number of channel paths in the system is given by $N^p_{i,j}$. Providing that BSs can receive measurements from UEs correctly and relay them to the CPU that performs the joint beamforming and power splitting (PS), the channel vector (CV) between BS i and UE j in time t can be obtained by

$$h_{i,j}[t] = \sqrt{\frac{\beta_{i,j}[t]}{N_{i,j}^p}} \sum_{p=1}^{N_{i,j}^p} \alpha_{i,j}^p[t] a\left(\phi_{i,j}^p\right)[t] \tag{1}$$

Further, as we focus on the DL context wherein BSs are transmitting to multiple UEs, the transmitted signal from BS i in time t can be represented by

$$x_i[t] = \sum_{j \in \mathbb{U}_i} \boldsymbol{\omega}_{i,j}[t] s_j \tag{2}$$

Here, $\boldsymbol{\omega}_{i,j}[t] \in \mathbb{C}^{M\text{BS}\times 1}$ denotes the DL beamforming vector (BV) between BS i and UE j in time t, while s_j is the data symbol for UE j. Given that, the received signal at UE j in time t can be written as

$$\Upsilon_j[t] = \sum_{i \in \mathbb{B}_j} \boldsymbol{h}_{i,j}^\dagger[t] \boldsymbol{\omega}_{i,j}[t] x_j[t] + \sum_{k \in \mathbb{U}\setminus j} \sum_{i \in \mathbb{B}_j} \boldsymbol{h}_{i,j}^\dagger[t] \boldsymbol{\omega}_{i,k}[t] x_k[t] + n_{A,j}[t] \tag{3}$$

In the above, $\boldsymbol{h}_{i,j}[t]$ is the CV just introduced in (1), and $n_{A,j} \sim \mathcal{CN}(0, \rho_{A,j}^2)$ denotes the additive complex Gaussian noise at UE j. Given that, the total received power at this UE in time t can be obtained by

$$P_j^r[t] = \sum_{k \in \mathbb{U}} \sum_{i \in \mathbb{B}_j} |\boldsymbol{h}_{i,j}^\dagger[t] \boldsymbol{\omega}_{i,k}[t]|^2 + \rho_{A,j}^2 \tag{4}$$

2.3 Nonlinear energy harvesting model

By means of SWIPT, each UE j can simultaneously perform ID and EH on the received signal $\Upsilon_j[t]$ with a PS scheme. Specifically, the PSR adopted by UE j is denoted by $\theta_j[t] \in (0, 1)$ as that in [43]. Further, a power splitter is introduced to divide the received power $P_j^r[t]$ into two flows. One of them is given by $(1-\theta_j)P_j^r$ and directed to the decoding block while the other is given by $\theta_j P_j^r$ and directed to the EH block, as shown in Fig. 1b. Consequently, the instantaneous SINR at UE j can be given by

$$\gamma_j[t] = \frac{\sum_{i \in \mathbb{B}_j} |\boldsymbol{h}_{i,j}^\dagger[t] \boldsymbol{\omega}_{i,j}[t]|^2}{\sum_{k \in \mathbb{U}\setminus j} \sum_{i \in \mathbb{B}_j} |\boldsymbol{h}_{i,j}^\dagger[t] \boldsymbol{\omega}_{i,k}[t]|^2 + \rho_{A,j}^2 + \frac{\rho_{I,j}^2}{1-\theta_j}} \tag{5}$$

where $\rho_{I,j}^2$ denotes the variance of random circuit noise for ID, $n_{I,j}$, in addition to $\rho_{A,j}^2$ just introduced. Given the SINR, the achievable data rate at UE j would be

$$R_j[t] = \log(1 + \gamma_j[t]) \tag{6}$$

However, unlike previous works, we consider the AC computing architecture in [35] and conduct another power splitter with a PSR ϕ_j to further divide the received power flow for EH into two parts. The first part, accounting for $1-\phi_j$ of this flow, is used to supply the AC computational logic, while the second part, with a proportion of ϕ_j, is dedicated to the energy management block, as shown in Fig. 1b as well. According to the power splits, the power to supply the AC computation at UE j can be given by

$$E_j^{\text{ac}} = \theta_j(1-\phi_j)\left(\sum_{k\in\mathbb{U}}\sum_{i\in\mathbb{B}_j}|\boldsymbol{h}_{i,j}^{\dagger}[t]\boldsymbol{\omega}_{i,k}[t]|^2 + \rho_{A,j}^2\right) \tag{7}$$

Similarly, with $\theta_j\phi_j$ of the power flow utilized to the DC energy for energy management, the EH for DC at UE j can be represented by [35]

$$E_j^{\text{dc}} = \frac{\frac{M^{\text{EH}}}{1+e^{-a(\widehat{\text{EH}}_j^{\text{dc}}-b)}} - \frac{M^{\text{EH}}}{1+e^{ab}}}{1-\frac{1}{1+e^{ab}}} \tag{8}$$

where $\widehat{\text{EH}}_j^{\text{dc}} = \theta_j\phi_j(\sum_{k\in\mathbb{U}}\sum_{i\in\mathbb{B}_j}|\boldsymbol{h}_{i,j}^{\dagger}[t]\boldsymbol{\omega}_{i,k}[t]|^2 + \rho_{A,j}^2)$, M^{EH} is the maximum harvested energy at a UE, and a and b are constants for circuit specification [44].

2.4 Cell-free problem formulation

Based on the above system model, our objective is to optimize BVs and PSRs in order to maximize the system sum-rate while ensuring that the energy allocated for the energy management block fulfils our demand. In addition, it needs to ensure that the DC harvested energy meets a specified requirement, and the transmit power of BSs remains within a bounded range. Specifically, the optimization problem can be formulated using the following programming model, despite the time index t:

$$(P0) \quad \max_{\boldsymbol{W},\boldsymbol{\Theta},\boldsymbol{\Phi}} \quad \sum_{j\in\mathbb{U}} R_j \tag{9a}$$

$$\text{subject to} \quad E_j^{\text{ac}} \geq \epsilon_{\text{ac}},\ \forall j \in \mathbb{U} \tag{9b}$$

$$E_j^{\text{dc}} \geq \epsilon_{\text{dc}},\ \forall j \in \mathbb{U} \tag{9c}$$

$$P_{\min} \leq \sum_{i\in\mathbb{B}_j}||\boldsymbol{\omega}_{i,j}||^2 \leq P_{\max},\ \forall j \in \mathbb{U} \tag{9d}$$

$$0 < \theta_j < 1,\ \forall j \in \mathbb{U} \tag{9e}$$

$$0 < \phi_j < 1,\ \forall j \in \mathbb{U} \tag{9f}$$

where $\boldsymbol{W}$ is the set of BVs ($\omega_{i,j}, \forall i \in \mathbb{B}_j, \forall j \in \mathbb{U}$), and $\boldsymbol{\Theta}$ and $\boldsymbol{\Phi}$ are the sets of PSRs (θ_j and $\phi_j, \forall j \in \mathbb{U}$), respectively. Given that, the first two sets of constraints, (9b) and (9c), specify the requirements that the energy allocated for the AC computational logic and that for the energy management block should be higher than ϵ_{ac} and ϵ_{dc}, respectively. Then, the set of constraints (9d) would ensure the transmit power of BVs to be bounded within $[P_{\min}, P_{\max}]$. Finally, the two sets constraints (9e) and (9f) simply denote that PRSs, θ_j and $\phi_j, \forall j \in \mathbb{U}$, should lie within the interval (0, 1).

3 Quadratic transform-based fractional programming algorithm for cell-free

As shown above, the optimization problem ($P0$) is intractable due to the coupling of variables $\boldsymbol{\omega}_{i,j}$, θ_j, and ϕ_j in the first two sets of constraints, resulting in a non-convex form. Additionally, the AC computing part introduces more variables and constraints compared to the linear EH model conventionally used. Given that, our objective is to efficiently address the problem ($P0$) in (9) and determine a feasible design for BVs ($\boldsymbol{W}$) and PRSs ($\boldsymbol{\Theta}$ and $\boldsymbol{\Phi}$) at each time t with low time complexity.

To this end, we first address the sum-logarithms present in the objective of optimization problem ($P0$) by employing the Lagrangian dual reformulation method in [45] to decouple the logarithms. Specifically, we have the following proposition:

Proposition 1 *By introducing a set of auxiliary variables,* $\boldsymbol{\xi} = \{\xi_1, \xi_2, \ldots, \xi_{N_u}\}$, *the optimization problem* (*P*0) *can be reformulated as*

$$\begin{aligned} &(P1)\ f(\boldsymbol{W}, \boldsymbol{\Theta}, \boldsymbol{\Phi}, \boldsymbol{\xi}) \\ &\quad \textbf{subjectto}\ \text{(9b), (9c), (9d), (9e), and (9f)} \end{aligned} \tag{10}$$

where the objective of (*P*1) *is*

$$f(\boldsymbol{W}, \boldsymbol{\Theta}, \boldsymbol{\Phi}, \boldsymbol{\xi}) = \sum_{j\in\mathbb{U}} \sum_{i\in\mathbb{B}_j} \left(\log(1+\xi_j) - \xi_j + (1+\xi_j) f_{i,j}(\boldsymbol{W}, \boldsymbol{\Theta}, \boldsymbol{\Phi}) \right) \tag{11}$$

In this objective, the function $f_{i,j}(\boldsymbol{W}, \boldsymbol{\Theta}, \boldsymbol{\Phi})$ *in the third term is*

$$f_{i,j}(\boldsymbol{W}, \boldsymbol{\Theta}, \boldsymbol{\Phi}) = \boldsymbol{\omega}_{i,j}^{\dagger} \boldsymbol{h}_{i,j} \left(\sum_{k\in\mathbb{U}} \boldsymbol{h}_{i,j}^{\dagger} \boldsymbol{\omega}_{i,k} (\boldsymbol{h}_{i,j}^{\dagger} \boldsymbol{\omega}_{i,k})^{\dagger} + \rho_{A,j}^2 + \frac{\rho_{I,j}^2}{1-\theta_j} \right)^{-1} \boldsymbol{h}_{i,j}^{\dagger} \boldsymbol{\omega}_{i,j} \tag{12}$$

With *Proposition* 1, we can then jointly optimize BVs and PSRs by solving the corresponding variables, $\boldsymbol{W}$, $\boldsymbol{\Theta}$, $\boldsymbol{\Phi}$, and $\boldsymbol{\xi}$, iteratively. For this, the optimization problem (*P*1) is divided into two subproblems and solved, respectively, as follows:

(1) Solve W **and** $\boldsymbol{\xi}$: First, by fixing $\boldsymbol{\Theta}$ and $\boldsymbol{\Phi}$ (represented by $\boldsymbol{\Theta}^*$ and $\boldsymbol{\Phi}^*$ here), the optimization problem (*P*1) can be reduced to P_{BV} for the BV design as

$$\begin{aligned} &(P_{\mathrm{BV}})\ \max_{\boldsymbol{W}}\ g_1(\boldsymbol{W}) = \sum_{j\in\mathbb{U}} \sum_{i\in\mathbb{B}_j} \nu_j f_{i,j}(\boldsymbol{W}, \boldsymbol{\Theta}^*, \boldsymbol{\Phi}^*) \\ &\quad \textbf{subjectto}\quad \text{(9b), (9c), and (9d)} \end{aligned} \tag{13}$$

where $\nu_j = 1 + \xi_j$. As shown readily, while (P_{BV}) appears to have a simpler form, $f_{i,j}$ in the objective is, in fact, a high-dimensional non-convex function as exhibited in (12). This function entails products of matrices and inverse matrices, and its non-convex nature is not easily mitigated by employing standard fractional programming methods, such as the classical Dinkelbach's transformation [46].

To resolve this issue, we turn to a recently proposed method, namely multidimensional complex quadratic transform (MCQT) [45], which expands scalar-form FP into a matrix-form framework, effectively tackling the challenge posed by high-dimensional non-convexity. Specifically, since $f_{i,j}$ in (12) fulfils the concave–convex conditions for MCQT, the problem (P_{BV}) can be reformulated through the following proposition:

Proposition 2 *By using the method of multidimensional complex quadratic transform* (*MCQT*) [45] *and introducing a set of auxiliary variables* $\boldsymbol{y} = [y_1, y_2, \ldots, y_{N_u}]$, *along with* $\hat{N}_j = j_{N_b} \times M_{\mathrm{BS}}$, *where* $j_{N_b} = \#\{\mathbb{B}_j\}$, *and* $\rho_j^2 = \rho_{A,j}^2 + \frac{\rho_{I,j}^2}{1-\theta_j}, \forall j \in \mathbb{U}$, *the optimization problem* (P_{BV}) *can be transformed to*

$$\begin{aligned} &(\widetilde{P}_{\mathrm{BV}})\ \max_{\boldsymbol{W},\boldsymbol{y}}\ g_2(\boldsymbol{W}, \boldsymbol{y}) \\ &\quad \textbf{subjectto}\quad \text{(9b), (9c), and (9d)} \end{aligned} \tag{14}$$

where

$$g_2(\boldsymbol{W},\boldsymbol{y}) = \sum_{j\in\mathbb{U}} \left(2\sqrt{\nu_j}\,\mathrm{Re}\left\{ \sum_{i\in\mathbb{B}_j} y_j^{\dagger}\boldsymbol{h}_{i,j}^{\dagger}\boldsymbol{\omega}_{i,j} \right\} - y_j^{\dagger}\left(\sum_{k\in\mathbb{U}}\sum_{i\in\mathbb{B}_k} \boldsymbol{h}_{i,j}^{\dagger}\boldsymbol{\omega}_{i,k}(\boldsymbol{h}_{i,j}^{\dagger}\boldsymbol{\omega}_{i,k})^{\dagger} + \rho_j^2\mathbf{I}_{\hat{N}_j} \right) y_j \right) \tag{15}$$

With the transformed quadratic form, we can update $\boldsymbol{W}$ and $\boldsymbol{\xi}$ (whose element ξ_j is shown in $\nu_j = 1+\xi_j$ in the above) along with $\boldsymbol{y}$ in turn, as follows: First, by fixing $\boldsymbol{W}$ and $\boldsymbol{\xi}$, in addition to the other variables, $\boldsymbol{\Theta}$ and $\boldsymbol{\Phi}$, to be fixed in this subproblem, we can solve $\frac{\partial g_2}{\partial y_j} = 0, \forall j \in \mathbb{U}$, with the first-order optimality to obtain the optimal

$$y_j^* = \left(\sum_{k\in\mathbb{U}}\sum_{i\in\mathbb{B}_k} \boldsymbol{h}_{i,j}^{\dagger}\boldsymbol{\omega}_{i,k}\boldsymbol{\omega}_{i,k}^{\dagger}\boldsymbol{h}_{i,j} + \rho_j^2\mathbf{I}_{\hat{N}_j} \right)^{-1} \left(\sqrt{\nu_j}\sum_{i\in\mathbb{B}_j} \boldsymbol{h}_{i,j}^{\dagger}\boldsymbol{\omega}_{i,j} \right) \tag{16}$$

Similarly, if $\boldsymbol{y}$ and $\boldsymbol{\xi}$ as well as $\boldsymbol{\Theta}$ and $\boldsymbol{\Phi}$ are fixed, the optimal $\boldsymbol{W}^*$, represented by its column-vector elements, $\overline{\omega}_j^* = \left\{ \omega_{i,j}^*, \forall i \in \mathbb{B}_j \right\}, \forall j \in \mathbb{U}$, can be given by

$$\overline{\omega}_j^* = \left(\sum_{k\in\mathbb{U}}\sum_{i\in\mathbb{B}_k} \boldsymbol{h}_{j,i}y_k y_k^{\dagger}\boldsymbol{h}_{j,i}^{\dagger} + \eta_j\mathbf{I}_{\hat{N}_j} \right)^{-1} \left(\sqrt{\nu_j}\sum_{i\in\mathbb{B}_j} \boldsymbol{h}_{i,j}y_j \right) \tag{17}$$

In the above, η_j is a dual variable introduced for the power constraint, which limits the power of BV to be within $[P_{\min}, P_{\max}]$. Here, we can efficiently find its optimal value

$$\eta_j^* = \min\left\{ \eta_j \geq 0 : P_{\min} \leq ||\overline{\omega}_j(\eta_j)||^2 \leq P_{\max} \right\} \tag{18}$$

by using a conventional bisection search method, where $\overline{\omega}_j = \left\{ \omega_{i,j}, \forall i \in \mathbb{B}_j \right\}, \forall j \in \mathbb{U}$.

On the other hand, by taking partial differentiation with respect to ξ_j in the objective $f(\boldsymbol{W},\boldsymbol{\Theta},\boldsymbol{\Phi},\boldsymbol{\xi})$ and solving $\frac{\partial f}{\partial \xi_j} = 0$, we can obtain its optimal, $\xi_j^*, \forall j \in \mathbb{U}$, as

$$\xi_j^* = \frac{\sum_{i\in\mathbb{B}_j} |\boldsymbol{h}_{i,j}^{\dagger}\boldsymbol{\omega}_{i,j}|^2}{\sum_{k\in\mathbb{U}\setminus j}\sum_{i\in\mathbb{B}_j} |\boldsymbol{h}_{i,j}^{\dagger}\boldsymbol{\omega}_{i,k}|^2 + \rho_{A,j}^2 + \frac{\rho_{I,j}^2}{1-\theta_j}} \tag{19}$$

Note that, although the third term of $f(\boldsymbol{W},\boldsymbol{\Theta},\boldsymbol{\Phi},\boldsymbol{\xi})$, i.e. $f_{i,j}(\boldsymbol{W},\boldsymbol{\Theta},\boldsymbol{\Phi})$ in (12), is similar to SINR in (5), its denominator involves desired signal, interferences, and noises, which is different from that of SINR. However, as shown in (19), the optimal auxiliary ξ_j^* is equal to SINR γ_j in (5), verifying the fact that the optimization problems ($P0$) and ($P1$) are equivalent, as exhibited in *Proposition* 1.

(2) Solve $\boldsymbol{\Theta}$ and $\boldsymbol{\Phi}$: Next, if $\boldsymbol{W}$ and $\boldsymbol{\xi}$ as well as $\boldsymbol{y}$ and $\boldsymbol{\eta}$ are given, the optimization problem $P0$ can be reduced to

$$(P2) \quad \max_{\boldsymbol{\Theta},\boldsymbol{\Phi}} \quad \sum_{j\in\mathbb{U}} R_j \qquad \textbf{subjectto} \quad (9b),\ (9c),\ (9e),\ \text{and } (9f) \tag{20}$$

Recall that $P_j^r = \sum_{k\in\mathbb{U}}\sum_{i\in\mathbb{B}_j} |\boldsymbol{h}_{i,j}^{\dagger}\boldsymbol{\omega}_{i,k}|^2 + \rho_{A,j}^2$ denotes the power received at UE j while ignoring the time index t, and let $\overline{\epsilon_{\mathrm{dc}}} = b - \frac{1}{a}\ln\left(\frac{e^{ab}(M^{\mathrm{EH}}-\epsilon_{\mathrm{dc}})}{e^{ab}\epsilon_{\mathrm{dc}}+M^{\mathrm{EH}}}\right)$ be the linear to nonlinear threshold transformation in [35]. In terms of the above, the first two constraints, (b) and (c), can be rewritten as

$$\theta_j(1-\phi_j)P_j^r \geq \epsilon_{\text{ac}} \tag{21}$$

$$\theta_j\phi_j P_j^r \geq \overline{\epsilon_{\text{dc}}} \tag{22}$$

In the reformulation, we can see that both requirements, $\theta_j \geq \frac{\epsilon_{\text{ac}}}{(1-\phi_j)P_j^r}$ and $\theta_j \geq \frac{\overline{\epsilon_{\text{dc}}}}{\phi_j P_j^r}$, should be satisfied at the same time. Thus, we require

$$\theta_j \geq \max\left\{\frac{\epsilon_{\text{ac}}}{(1-\phi_j)P_j^r}, \frac{\overline{\epsilon_{\text{dc}}}}{\phi_j P_j^r}\right\} \tag{23}$$

where ϕ_j is bounded within (0, 1), and the objective function in the right-hand side is in the form of $\max\left\{f(\frac{1}{(1-\phi_j)}), g(\frac{1}{\phi_j})\right\}$. As noted in [35], the optimal ϕ_j^* in this form would satisfy the condition:

$$\frac{\epsilon_{\text{ac}}}{(1-\phi_j^*)P_j^r} = \frac{\overline{\epsilon_{\text{dc}}}}{\phi_j^* P_j^r} \tag{24}$$

Accordingly, the optimal EH can be obtained in terms of

$$\phi_j^* = \phi^* = \frac{\overline{\epsilon_{\text{dc}}}}{\epsilon_{\text{ac}} + \overline{\epsilon_{\text{dc}}}} \tag{25}$$

Next, we substitute ϕ_j in ($P2$) with ϕ^* to find θ_j^*. Specifically, if the optimal $\theta_j^* = \theta^*, \forall j \in \mathbb{U}$, and, without loss of generality, along with the given ϕ_j^*, we can transform the optimization problem ($P2$) into a one-dimensional search problem on θ, as follows:

$$(P3) \quad \arg\max_{\theta} \quad \sum_{j\in\mathbb{U}} R_j \tag{26a}$$

$$\textbf{subjectto} \quad \theta(1-\phi^*)P_j^r \geq \epsilon_{\text{ac}}, \ \forall j \in \mathbb{U} \tag{26b}$$

$$\theta\phi^* P_j^r \geq \overline{\epsilon_{\text{dc}}}, \ \forall j \in \mathbb{U} \tag{26c}$$

which can be solved with an initial feasible value.

Time complexity In summary, the quadratic transform-based FP algorithm dedicated to cell-free massive MIMO can solve problem $P0$ in (9) by iteratively updating the optimal $\boldsymbol{y}$, $\boldsymbol{\xi}$, $\boldsymbol{W}$, $\boldsymbol{\Theta}$, and $\boldsymbol{\Phi}$. Its pseudocode is now shown in Algorithm 1 for easy reference. Note that, in each of $\mathcal{L}_m$ iterations at most, an inverse operation is required to find $\overline{\omega}_j^*$ with $O((N_u M_{\text{BS}})^3)$ time for each column-vector element $j \in \mathbb{U}$, where $N_u = \#\{\mathbb{U}\}$ is the number of UEs in $\mathbb{U}$ as defined. Further, the number of $\mathcal{L}_\eta$ bisection-search iterations at most is also required to find η_j^* along with the above for $\overline{\omega}_j^*$ as shown in line 5. In addition, the one-dimensional search for θ^* can be solved in $O(L_\theta)$ time, where L_θ is the length of the search interval (0, 1) for θ. Apart from the above, the other parameters can be easily obtained through the corresponding closed-form solutions. Consequently, the overall time complexity could be estimated as $O(\mathcal{L}_m(\mathcal{L}_\eta(N_u(N_u M_{\text{BS}})^3) + L_\theta))$ or simply $O(\mathcal{L}_m\mathcal{L}_\eta N_u^4 M_{\text{BS}}^3)$ if $O(L_\theta)$ could be ignored when compared with $O(\mathcal{L}_\eta N_u(N_u M_{\text{BS}})^3)$ in the worst-time complexity analysis.

Algorithm 1 The quadratic transform-based FP Algorithm for cell-free massive MIMO

Set $c_m = 0$ and $c_\eta = 0$;
Initialize $\mathcal{L}_m$, $\mathcal{L}_\eta$, $\boldsymbol{y}, \boldsymbol{\xi}, \boldsymbol{W}, \boldsymbol{\Theta}$, and $\boldsymbol{\Phi}$ to feasible values;
repeat
  Update $y_j^*, \forall j$, with (16), while fixing $\boldsymbol{W}$, $\boldsymbol{\Theta}$, $\boldsymbol{\Phi}$, and $\boldsymbol{\xi}$;
  Update $\overline{\omega}_j^*, \forall j$, with (17) and find $\eta_j^*, \forall j$, in (18) iteratively by using a bisection search which increases c_η by 1 during each of its own iterations until convergence or $c_\eta > \mathcal{L}_\eta$, while fixing $\boldsymbol{y}$, $\boldsymbol{\Theta}$, $\boldsymbol{\Phi}$, and $\boldsymbol{\xi}$;
  Update $\xi_j^*, \forall j$, with (19), while fixing $\boldsymbol{y}$, $\boldsymbol{W}$, $\boldsymbol{\Theta}$, and $\boldsymbol{\Phi}$;
  Update ϕ^* with (25), while fixing $\boldsymbol{y}$, $\boldsymbol{\xi}$, $\boldsymbol{W}$, and $\boldsymbol{\Theta}$;
  Update θ^* by solving $(P3)$ with a one-dimensional search algorithm while fixing $\boldsymbol{y}$, $\boldsymbol{\xi}$, $\boldsymbol{W}$, and $\boldsymbol{\Phi}$;
  $c_m = c_m + 1$;
until convergence or $c_m > \mathcal{L}_m$

4 Sequential beamforming and power splitting algorithm for cell-free

As can be seen readily, the non-convex BV optimization is the most time-consuming step in solving problem ($P0$), and the proposed FP-based algorithm can effectively reduce its time complexity. However, to further reduce the complexity, we incorporate conventional beamforming schemes such as ZF, MRT, and SLNR as alternatives to the search for optimal BV. This results in a sequential beamforming and power splitting algorithm that is sufficiently time-efficient for real-time operations. That is, despite $\boldsymbol{\Theta}$ and $\boldsymbol{\Phi}$, the optimization problem ($P0$) can be reduced to focus on $\boldsymbol{W}$, as

$$
\begin{aligned}
(P4) \quad & \max_{\boldsymbol{W}} && \textstyle\sum_{j\in\mathbb{U}} R_j && \text{(27a)}\\
& \textbf{subjectto} && E_j^{\mathrm{ac}} \geq \epsilon_{\mathrm{ac}},\ \forall j \in \mathbb{U} && \text{(27b)}\\
& && E_j^{\mathrm{dc}} \geq \epsilon_{\mathrm{dc}},\ \forall j \in \mathbb{U} && \text{(27c)}\\
& && P_{\min} \leq \textstyle\sum_{i\in\mathbb{B}_j} ||\boldsymbol{\omega}_{i,j}||^2 \leq P_{\max},\ \forall j \in \mathbb{U} && \text{(27d)}
\end{aligned}
$$

When compared with ($P0$), this problem exhibits a simpler programming model. However, as noted before, it remains non-convex due to the maximization objective, which includes logarithmic functions with inputs of SINR represented as a ratio of two quadratic terms. Therefore, in addition to the introduced FP method, considering conventional beamforming schemes provides an alternative to implement a simpler yet more time-efficient sequential algorithm.

4.1 ZF beamforming

In convention, zero-forcing (ZF) is utilized to cancel the cross-interference links by using appropriate BVs. For cell-free massive MIMO, the condition for ZF BV $\boldsymbol{\omega}_{i,j}$ can be written as $\boldsymbol{h}_{i',j}^\dagger \boldsymbol{\omega}_{i,j} = 0, \forall i' \in \mathbb{B}\backslash i$, while maximizing $||\boldsymbol{h}_{i,j}^\dagger \boldsymbol{\omega}_{i,j}||^2$. More specifically, the optimization problem with respect to ZF can be formulated as

$$
\begin{aligned}
(P^{\mathrm{ZF}}) \quad & \max_{\boldsymbol{\omega}_{i,j}} && ||\boldsymbol{h}_{i,j}^\dagger \boldsymbol{\omega}_{i,j}||^2 && \text{(28a)}\\
& \textbf{subjectto} && E_j^{\mathrm{ac}} \geq \epsilon_{\mathrm{ac}}, && \text{(28b)}\\
& && \boldsymbol{H}_{i,j}^\dagger \boldsymbol{\omega}_{i,j} = 0, && \text{(28c)}\\
& && 0 \leq ||\boldsymbol{\omega}_{i,j}||^2 \leq 1, && \text{(28d)}
\end{aligned}
$$

where $\boldsymbol{H}_{i,j}$ is the set of channels $\{\boldsymbol{h}_{i',j}, \forall i' \in \mathbb{B}\backslash i\}$ for link $\{i,j\}$, and the transmit power $||\boldsymbol{\omega}_{i,j}||^2$ is normalized to the unit range [0, 1] to obtain the ZF BV as

$$\boldsymbol{\omega}_{i,j}^{\mathrm{ZF}} = \frac{\left(\mathbf{I}_{M_{\mathrm{BS}}} - \boldsymbol{H}_{i,j}^{+}\boldsymbol{H}_{i,j}\right)\boldsymbol{h}_{i,j}^{\dagger}}{||\left(\mathbf{I}_{M_{\mathrm{BS}}} - \boldsymbol{H}_{i,j}^{+}\boldsymbol{H}_{i,j}\right)\boldsymbol{h}_{i,j}^{\dagger}||} \tag{29}$$

4.2 MRT beamforming

Unlike ZF, which focuses on interference cancellation, maximum ratio transmission (MRT) is another widely used technique in wireless communication that aims to enhance the received signal quality. MRT achieves this by scaling the transmitted signal based on the ratio of the channel coefficients, resulting in an improved signal-to-noise ratio (SNR) at receiver. Specifically, without considering interference, the MRT BV can be easily realized by

$$\boldsymbol{\omega}_{i,j}^{\mathrm{MRT}} = \frac{\boldsymbol{h}_{i,j}^{\star}}{||\boldsymbol{h}_{i,j}^{\star}||} \tag{30}$$

Note that, in the conventional sense of ID, this algorithm may result in strong cross-interference because it does not consider simultaneous transmissions. However, for SWIPT, it could exhibit different characteristics in terms of EH, in addition to those expected for ID, which will be revealed in our simulation study.

4.3 SLNR beamforming

When compared with SINR adopted in Sect. 3, signal-to-leakage-and-noise ratio (SLNR) has the benefit to avoid collecting channel information from other stations. Hence, it usually serves as a convenient alternative to SINR, especially when obtaining such information poses challenges for local stations. Specifically, SLNR is defined as the ratio between the transmitted power to the desired UE and that leaked to other unintended UEs, as

$$\beta_{i,j} = \frac{|\boldsymbol{h}_{i,j}^{\dagger}\boldsymbol{\omega}_{i,j}|^2}{\sum_{k\in\mathbb{U}_i\backslash j}|\boldsymbol{h}_{i,k}^{\dagger}\boldsymbol{\omega}_{i,j}|^2 + \rho_j^2} \tag{31}$$

Here, by adding the notation $\tilde{\boldsymbol{H}}_{i,j}$ to denote the set of channels $\{\boldsymbol{h}_{i,j}, \forall i \in \mathbb{B}\}$ for link $\{i,j\}$, we can obtain the SLNR BV in this scenario, based on [47], as

$$\boldsymbol{\omega}_{i,j}^{\mathrm{SLNR}} = \frac{\left(\rho_j^2\mathbf{I}_{M_{\mathrm{BS}}} + \tilde{\boldsymbol{H}}_{i,j}^{\dagger}\tilde{\boldsymbol{H}}_{i,j}\right)^{-1}\boldsymbol{h}_{i,j}}{||\left(\rho_j^2\mathbf{I}_{M_{\mathrm{BS}}} + \tilde{\boldsymbol{H}}_{i,j}^{\dagger}\tilde{\boldsymbol{H}}_{i,j}\right)^{-1}\boldsymbol{h}_{i,j}||} \tag{32}$$

Note that the BVs obtained in the above, i.e. $\boldsymbol{\omega}_{i,j}^{\mathrm{ZF}}$, $\boldsymbol{\omega}_{i,j}^{\mathrm{MRT}}$ and $\boldsymbol{\omega}_{i,j}^{\mathrm{SLNR}}$, should be scaled back to ensure that $\sum_{j\in\mathbb{U}}||\boldsymbol{\omega}_{i,j}^{M}||^2, \forall i$, where M represents the method of ZF, MRT, or SLNR, remains within the original bound $[P_{\min}, P_{\max}]$.

Algorithm 2 The sequential beamforming and power splitting algorithm for cell-free massive MIMO

for $i = 1$ to N_b **do**
  for $j = 1$ to N_u **do**
    if BS i serves UE j **then**
      Obtain $\omega_{i,j}^{ZF}$, $\omega_{i,j}^{MRT}$, or $\omega_{i,j}^{SLNR}$, with (29), (30), or (32);
    end if
  end for
end for
Obtain ϕ^* with (25);
Obtain θ^* by solving $(P3)$ with a one-dimensional search algorithm, given $\boldsymbol{W}$ composed of $\omega_{i,j}^{ZF}$, $\omega_{i,j}^{MRT}$, or $\omega_{i,j}^{ZF}$, $\forall i, \forall j$;

Time complexity Given these beamforming schemes, which provide $\boldsymbol{W}$ without finding $\boldsymbol{\xi}$ in Algorithm 1, the remaining PSR problem can be solved with the same way to find $\boldsymbol{\Theta}^*$ and $\boldsymbol{\Phi}^*$ in Sect. 3. As a summary, the overall sequential beamforming and power splitting algorithm for cell-free massive MIMO is tabulated in Algorithm 2 for easy reference. As exhibited therein, this algorithm first requires $O(N_b N_u)$ to find BVs. Then, it needs $O(L_\theta)$ time to find PSRs with the one-dimensional search as that in Algorithm 1. Thus, its time complexity could be estimated as $O(N_b N_u + L_\theta)$.

5 Small-cell modelling and problem formulation

5.1 System Model

To align with the cell-free environment, the DL wireless network is considered to comprise N_b cells, with each cell containing a BS equipped with M_{BS} antennas for transmitting to a single-antenna UE, as shown in Fig. 2. In addition, each cell can support multiple UEs by utilizing orthogonal frequency bands, thereby avoiding intra-cell interference. However, because there could be a frequency band adopted by, say UE i (served by BS i), to be shared by other BSs $k \in \mathbb{B}_i \backslash i$, inter-cell interference is still possible. Therefore, when analysing a specific frequency band, we can model the channel of this system as a multi-cell multiple-input single-output interference channel (MISO-IC). Specifically, in the context of a specific orthogonal frequency band, each BS i can pre-code the transmitted signal $\hat{x}_i$ with its BV, $\hat{\boldsymbol{\omega}}_i$, to communicate with the intended UE i. Consequently, the received signal at UE i can be formulated as

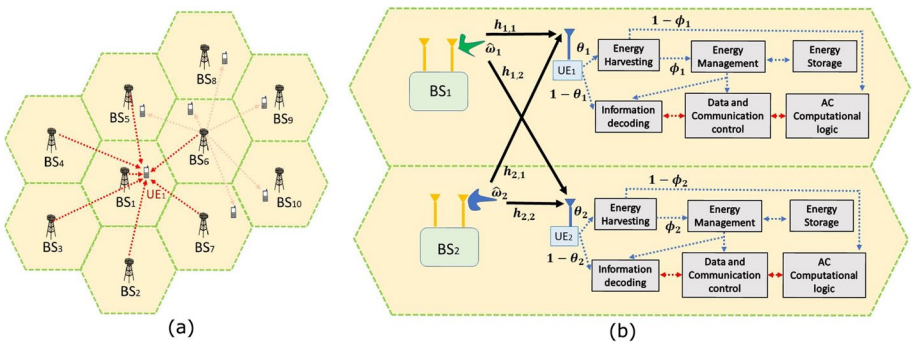

Fig. 2 Small-cell network: **a** topology layout, and **b** SWIPT system with integrate ID and EH (a two-BSs example)

$$\hat{\Upsilon}_i = \boldsymbol{h}_{i,i}^{\dagger}\hat{\boldsymbol{\omega}}_i\hat{x}_i + \sum_{k\in\mathbb{B}_i\setminus i}\boldsymbol{h}_{k,i}^{\dagger}\hat{\boldsymbol{\omega}}_k\hat{x}_k + n_i \tag{33}$$

Note that, unlike in the previous cell-free scenario wherein a CPU can assist in determining $\boldsymbol{\omega}_{i,j}$ between BS i and UE j, in the small-cell scenario, each BS i can only conduct its $\hat{\omega}_i$ towards its intended UE i on a specific band, without further coordination to decide BVs towards UEs in other cells.

Given that, the SINR at UE i can be given by

$$\hat{\gamma}_i = \frac{|\boldsymbol{h}_{i,i}^{\dagger}\hat{\boldsymbol{\omega}}_i|^2}{\sum_{k\in\mathbb{B}_i\setminus i}|\boldsymbol{h}_{k,i}^{\dagger}\hat{\boldsymbol{\omega}}_k|^2 + \rho_{A,i}^2 + \frac{\rho_{I,i}^2}{1-\theta_i}} \tag{34}$$

With this SINR, the achievable data rate at UE i in the small-cell scenario can be denoted by

$$\hat{R}_i = \log(1+\hat{\gamma}_i) \tag{35}$$

Similarly, with the nonlinear EH model in Sect. 2.3, the power to supply the AC computation at UE i in this scenario can be given by

$$\hat{E}_i^{\mathrm{ac}} = \theta_i(1-\phi_i)\left(\sum_k |\boldsymbol{h}_{k,i}^{\dagger}\hat{\boldsymbol{\omega}}_k|^2 + \rho_{A,i}^2\right) \tag{36}$$

Further, with $\widetilde{\mathrm{EH}}_i^{dc} = \theta_i\phi_i(\sum_k |\boldsymbol{h}_{k,i}^{\dagger}\hat{\boldsymbol{\omega}}_k|^2 + \rho_{A,i}^2)$, the EH for DC at UE i would be represented by

$$\hat{E}_i^{dc} = \frac{\frac{M^{\mathrm{EH}}}{1+e^{-a(\widetilde{\mathrm{EH}}_i^{dc}-b)}} - \frac{M^{\mathrm{EH}}}{1+e^{ab}}}{1-\frac{1}{1+e^{ab}}} \tag{37}$$

5.2 Problem formulation

As with the case of cell-free communication, our goal in the small-cell scenario is to optimize BVs and PSRs so that the system sum-rate can be maximized, subject to the constraints on harvested energy, AC logic energy supply, and total transmit power, as well. However, by denoting $\widehat{\boldsymbol{W}}$ as the set of BVs ($\hat{\omega}_i, \forall i$), and $\widehat{\boldsymbol{\Theta}}$ and $\widehat{\boldsymbol{\Phi}}$ as the sets of PSRs ($\hat{\theta}_i$ and $\hat{\phi}_i$, $\forall i$), which are specific to the small-cell scenario, the optimization problem gains its distinct characteristics and can be formulated as:

$$(P5)\quad \max_{\widehat{\boldsymbol{W}},\widehat{\boldsymbol{\Theta}},\widehat{\boldsymbol{\Phi}}} \quad \sum_i \hat{R}_i \tag{38a}$$

$$\textbf{subjectto} \quad \hat{E}_i^{\mathrm{ac}} \geq \epsilon_{\mathrm{ac}}, \quad \forall i \tag{38b}$$

$$\hat{E}_i^{dc} \geq \epsilon_{dc}, \quad \forall i \tag{38c}$$

$$P_{\min} \leq ||\hat{\boldsymbol{\omega}}_i||^2 \leq P_{\max} \quad \forall i \tag{38d}$$

$$0 < \hat{\theta}_i < 1, \quad \forall i \tag{38e}$$

$$0 < \hat{\phi}_i < 1, \quad \forall i \tag{38f}$$

6 Quadratic transform-based fractional programming algorithm for small-cell

For this scenario, we can similarly adopt the Lagrangian dual reformulation with a set of auxiliary variables $\widehat{\boldsymbol{\xi}} = \left\{\hat{\xi}_1, \hat{\xi}_2, \ldots, \hat{\xi}_{N_b}\right\}$, and according to the MCQT method, rewrite the objective of (*P*5) to

$$\textbf{max} \;\; \hat{f} = \sum_i \left(\log(1+\hat{\xi}_i) - \hat{\xi}_i + \frac{(1+\hat{\xi}_i)|\boldsymbol{h}_{i,i}^{\dagger}\hat{\boldsymbol{\omega}}_i|^2}{\sum_{k\in\mathbb{B}_i\setminus i}|\boldsymbol{h}_{k,i}^{\dagger}\hat{\boldsymbol{\omega}}_k|^2+\rho_i^2} \right) \tag{39}$$

where $\rho_i^2 = \rho_{A,i}^2 + \frac{\rho_{I,i}^2}{1-\theta_i}, \forall i$. Then, by applying the first-order optimality to $\hat{f}$ for $\widehat{\boldsymbol{\xi}}$, i.e. solving $\frac{\partial \hat{f}}{\partial \hat{\xi}_i} = 0, \forall i$, we can obtain

$$\hat{\xi}_i^* = \frac{|\boldsymbol{h}_{i,i}^{\dagger}\hat{\boldsymbol{\omega}}_i|^2}{\sum_{k\in\mathbb{B}_i\setminus i}|\boldsymbol{h}_{k,i}^{\dagger}\hat{\boldsymbol{\omega}}_k|^2+\rho_i^2} \tag{40}$$

which is equal to the SINR for the small-cell scenario. That is, the two objectives (38a) and (39) are equivalent. Given that, we can similarly apply the MCQT method, similarly to that in *Proposition* 2, to the latter, i.e. (39), resulting in the transformed objective,

$$\textbf{max}\hat{Q} = \sum_i \left(2\sqrt{\hat{\nu}_i}\,\mathrm{Re}\left\{\hat{y}_i^{\dagger}\boldsymbol{h}_{i,i}^{\dagger}\hat{\boldsymbol{\omega}}_i\right\} - \hat{y}_i^{\dagger}\left(\sum_{k\in\mathbb{B}_i\setminus i} \boldsymbol{h}_{k,i}^{\dagger}\hat{\boldsymbol{\omega}}_k(\boldsymbol{h}_{k,i}^{\dagger}\hat{\boldsymbol{\omega}}_k)^{\dagger} + \rho_i^2\mathbf{I}_{M_{\mathrm{BS}}} \right)\hat{y}_i \right) \tag{41}$$

where $\hat{\nu}_i$ represents $1+\hat{\xi}_i$, and $\widehat{\boldsymbol{y}} = [\hat{y}_1, \hat{y}_2, \ldots, \hat{y}_{N_b}]$ denotes a set of auxiliary variables for the small-cell scenario. Then, to find its optimal value, we can solve $\frac{\partial \hat{Q}}{\partial \hat{y}_i} = 0, \forall i$, with fixed $\widehat{\boldsymbol{W}}$, $\widehat{\boldsymbol{\Theta}}$, $\widehat{\boldsymbol{\Phi}}$, and $\widehat{\boldsymbol{\xi}}$, resulting in

$$\hat{y}_i^* = \left(\sum_{k\in\mathbb{B}_i\setminus i} \boldsymbol{h}_{k,i}^{\dagger}\hat{\boldsymbol{\omega}}_k\hat{\boldsymbol{\omega}}_k^{\dagger}\boldsymbol{h}_{k,i} + \rho_i^2\mathbf{I}_{M_{\mathrm{BS}}} \right)^{-1} \left(\sqrt{\hat{\nu}_i}\boldsymbol{h}_{i,i}^{\dagger}\hat{\boldsymbol{\omega}}_i \right) \tag{42}$$

Similarly, with fixed $\widehat{\boldsymbol{y}}$, $\widehat{\boldsymbol{\Theta}}$, $\widehat{\boldsymbol{\Phi}}$, and $\widehat{\boldsymbol{\xi}}$, the optimal $\widehat{\boldsymbol{W}}^*$, comprising $\hat{\omega}_i^*, \forall i$, can be obtained by

$$\hat{\omega}_i^* = \left(\sum_{k\in\mathbb{B}_i\setminus i} \boldsymbol{h}_{i,k}\hat{y}_k\hat{y}_k^{\dagger}\boldsymbol{h}_{i,k}^{\dagger} + \hat{\eta}_i\mathbf{I}_{M_{\mathrm{BS}}} \right)^{-1} \left(\sqrt{\hat{\nu}_i}\boldsymbol{h}_{i,i}\hat{y}_i \right) \tag{43}$$

where $\hat{\eta}_i$ is a dual variable introduced for the power constraint in the small-cell scenario, which can be similarly obtained by using a bisection search method.

Algorithm 3 The quadratic transform-based FP Algorithm for small-cell

1: Set $\hat{c}_m = 0$ and $\hat{c}_\eta = 0$;
2: Initialize $\hat{\mathcal{L}}_m$, $\hat{\mathcal{L}}_\eta$, $\widehat{\boldsymbol{y}}, \widehat{\boldsymbol{\xi}}, \widehat{\boldsymbol{W}}, \widehat{\boldsymbol{\Theta}}$, and $\widehat{\boldsymbol{\Phi}}$ to feasible values;
3: **repeat**
4: Update $\hat{y}_i^*, \forall i$, with (42), while fixing $\widehat{\boldsymbol{W}}$, $\widehat{\boldsymbol{\Theta}}$, $\widehat{\boldsymbol{\Phi}}$, and $\widehat{\boldsymbol{\xi}}$;
5: Update $\hat{\omega}_i^*, \forall i$, with (43) and find the corresponding $\eta_i^*, \forall i$, iteratively, with a bisection search similar to that given in Sect. 3 when $\hat{c}_\eta{+}{+} < \hat{\mathcal{L}}_\eta$, while fixing $\widehat{\boldsymbol{y}}$, $\widehat{\boldsymbol{\Theta}}$, $\widehat{\boldsymbol{\Phi}}$, and $\widehat{\boldsymbol{\xi}}$;
6: Update $\xi_i^*, \forall i$, with (40), while fixing $\widehat{\boldsymbol{y}}$, $\widehat{\boldsymbol{W}}$, $\widehat{\boldsymbol{\Theta}}$, and $\widehat{\boldsymbol{\Phi}}$;
7: Update $\hat{\phi}^*$ with a closed-form solution similar to (25), while fixing $\widehat{\boldsymbol{y}}$, $\widehat{\boldsymbol{\xi}}$, $\widehat{\boldsymbol{W}}$, and $\widehat{\boldsymbol{\Theta}}$;
8: Update $\hat{\theta}^*$ by solving a reduced problem similar to (*P*3) with a one-dimensional search algorithm like that in Sect. 3, while fixing $\widehat{\boldsymbol{y}}$, $\widehat{\boldsymbol{\xi}}$, $\widehat{\boldsymbol{W}}$, and $\widehat{\boldsymbol{\Phi}}$;
9: **until** convergence or $\hat{c}_m{+}{+} > \hat{\mathcal{L}_m}$

Apart from the above for $\widehat{\boldsymbol{W}}$ and $\widehat{\boldsymbol{\xi}}$, the steps to obtain the optimal values for $\widehat{\boldsymbol{\Theta}}$ and $\widehat{\boldsymbol{\Phi}}$ can be done like that shown in Sect. 3. Finally, we present the FP-based algorithm for the small-cell scenario in Algorithm 3 for easy reference.

7 Sequential beamforming and power splitting algorithm for small-cell

For the small-cell scenario, when $\widehat{\boldsymbol{\Theta}}$ and $\widehat{\boldsymbol{\Phi}}$ are not considered, the optimization problem ($P5$) can be reduced to

$$
\begin{aligned}
(P6) \quad \max_{\widehat{\boldsymbol{W}}} \quad & \textstyle\sum_i \hat{R}_i && && (44a)\\
\textbf{subjectto} \quad & \hat{E}_i^{\mathrm{ac}} \geq \epsilon_{\mathrm{ac}}, && \forall i && (44b)\\
& \hat{E}_i^{dc} \geq \epsilon_{dc}, && \forall i && (44c)\\
& P_{\min} \leq ||\hat{\boldsymbol{\omega}}_i||^2 \leq P_{max}, && \forall i && (44d)
\end{aligned}
$$

For this problem, $\hat{\boldsymbol{H}}_i$ denotes the set of channels, $\{h_{k,i}, \forall k \in \mathbb{B}_i \backslash i\}$, and $\mathbb{B}_i$ represents the set of BSs that can interfere with UE i rather than serve it in the cell-free scenario. Additionally, the transmit power $||\hat{\boldsymbol{\omega}}_i||^2$ is normalized to the unit range [0, 1] as before. Given that, the ZF BV for the small-cell scenario can be obtained by

$$
\hat{\boldsymbol{\omega}}_i^{\mathrm{ZF}} = \frac{\left(\mathbf{I}_{M_{\mathrm{BS}}} - \hat{\boldsymbol{H}}_i^{+}\hat{\boldsymbol{H}}_i\right)\boldsymbol{h}_{i,i}^{\dagger}}{||\left(\mathbf{I}_{M_{\mathrm{BS}}} - \hat{\boldsymbol{H}}_i^{+}\hat{\boldsymbol{H}}_i\right)\boldsymbol{h}_{i,i}^{\dagger}||} \tag{45}
$$

Similarly, by focusing on SNR and ignoring cross-interference as before, the MRT BV can be realized in this scenario as

$$
\hat{\boldsymbol{\omega}}_i^{\mathrm{MRT}} = \frac{\boldsymbol{h}_{i,i}^{\star}}{||\boldsymbol{h}_{i,i}^{\star}||} \tag{46}
$$

At last, in terms of $\check{\boldsymbol{H}}_i$ that represents the set of channels, $\{h_{k,i}, \forall k \in \mathbb{B}_i\}$, the SLNR BV for the small-cell scenario can be determined by

$$
\hat{\boldsymbol{\omega}}_i^{\mathrm{SLNR}} = \frac{(\rho_i^2\mathbf{I}_{M_{\mathrm{BS}}} + \check{\boldsymbol{H}}_i^{\dagger}\check{\boldsymbol{H}}_i)^{-1}\boldsymbol{h}_{i,i}}{||(\rho_i^2\mathbf{I}_{M_{\mathrm{BS}}} + \check{\boldsymbol{H}}_i^{\dagger}\check{\boldsymbol{H}}_i)^{-1}\boldsymbol{h}_{i,i}||} \tag{47}
$$

Note that these BVs ($\hat{\boldsymbol{\omega}}_i^{\mathrm{ZF}}$, $\hat{\boldsymbol{\omega}}_i^{\mathrm{MRT}}$, and $\hat{\boldsymbol{\omega}}_i^{\mathrm{SLNR}}$) would then be scaled back to make $||\hat{\boldsymbol{\omega}}_i^{M}||^2, \forall i$, where $M \in \{$ ZF, MRT, SLNR $\}$, within the original range $[P_{\min}, P_{max}]$.

Algorithm 4 The sequential beamforming and power splitting algorithm for small-cell

1: **for** $i = 1$ to N_b **do**
2: Obtain $\hat{\omega}_i^{ZF}$, $\hat{\omega}_i^{MRT}$, or $\hat{\omega}_i^{SLNR}$, with (45), (46), or (47);
3: **end for**
4: Obtain $\hat{\phi}^*$ with an equation similar to (25);
5: Obtain $\hat{\theta}^*$ by solving a reduced problem similar to ($P3$) with a one-dimensional search algorithm like that in Sect. 3, given $\widehat{\boldsymbol{W}}$ composed of $\hat{\omega}_i^{ZF}$, $\hat{\omega}_i^{MRT}$, or $\hat{\omega}_i^{ZF}, \forall i$;

After addressing the BV issue, the PSR problem for the small-cell scenario can be similarly solved as described in Sect. 3 to find the optimal values for $\widehat{\boldsymbol{\Theta}}$ and $\widehat{\boldsymbol{\Phi}}$. Finally, the overall sequential beamforming and power splitting algorithm for this scenario is summarized in Algorithm 4 for easy reference.

8 Results and discussion

In this section, we conduct simulation experiments to evaluate the performance of the algorithms developed for the cell-free mass MIMO networks and the small-cell networks, respectively. To this end, the simulation environment is first introduced. Then, rate-energy representations, also known as rate-energy regions, are used to illustrate the trade-off between the system sum-rate and the amount of EH realized by the different algorithms proposed. In addition, we also include the approximation solution for the max–min power control with ZF beamforming proposed in [29]. This method represents a low-complexity solution with conventional beamforming in the literature. However, it does not provide a solution for the PSR problem in the SWIPT system. Thus, we randomly generate a PSR after applying this method. The resulting algorithm is called 'ZF-APX' and serves as a baseline algorithm for the sequel.

Given that, the two metrics are evaluated by varying the transmit power of BSs, and the number of cells in the system, respectively, for each of the algorithms. Through the evaluation, the performance differences of these algorithms considering both ID and EH are revealed, showcasing their characteristics and providing insights that were not previously explored in works focusing solely on ID in these networks. While showing this, we would use *'cell-free scenario'* and *'small-cell scenario'* to refer to *'cell-free massive MIMO network'* and *'small-cell network'*, respectively, for easy of notation, whenever there is no confusion.

8.1 Simulation setup

By considering both system models introduced Sects. 2.1 and 5.1, we conduct the simulation environment as shown in Fig. 3 to have 19 hexagonal cells with BS 0 located at the centre, BSs 1–6 located in the first tier, and BSs 7–18 located in the second tier, similar to the environment in [48] but with different radio parameters. In the cell-free scenario, the same BSs are considered to serve the corresponding UEs as in the multi-cell environment. However, it has no cell boundaries in this scenario, which results in a similar configuration for fair comparison. In addition, it is assumed that $\mathbb{B}_i = \mathbb{B}, \forall i$, and $\mathbb{U}_i = \mathbb{U}, \forall i$, in the simulation study, without loss of generality. Here, the simulation codes are developed on PYTHON [49] which calls MATLAB [50] to obtain the BVs involved and are executed on a 64-bit operating system with 16 GB RAM and Intel CORE i9, 5.5 GHz.

Furthermore, to simulate the conditions of a small cell where significant energy harvesting is possible in addition to data transmission, the cell radius is limited to 20 m for SWIPT. Each UE is randomly located within each cell, and the path loss between BS i and UE j is proportional to $d_{i,j}^{-k}$, where the distance between them, $d_{j,k}$, is measured in kilometres, and $k = 3$ is the path loss exponent. Apart from the above, the energy

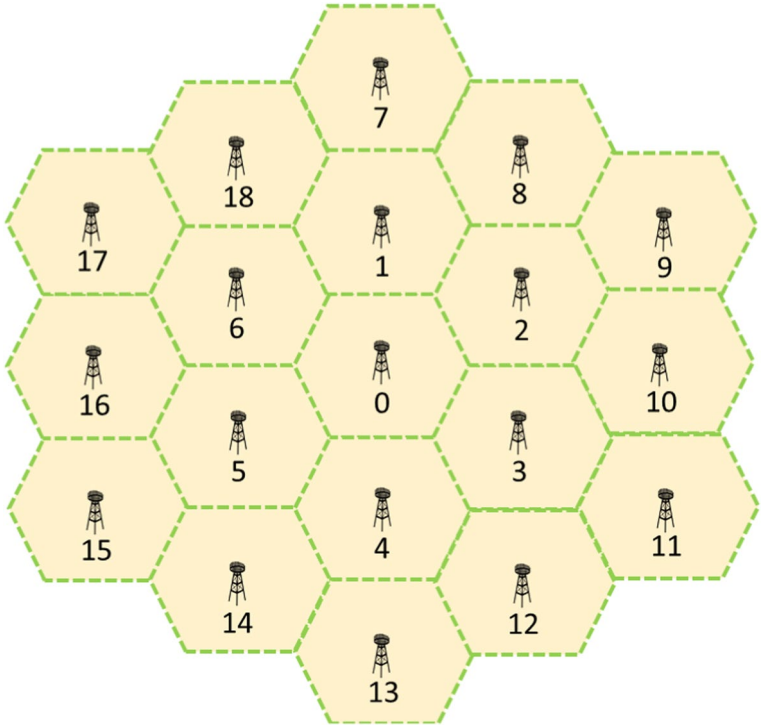

Fig. 3 Simulation topology, similar to that in [48]

requirements or thresholds are given as $\epsilon_{ae} = 0.04764$ mW and $\epsilon_{de} = 0.2$ mW as that in [35], and the maximum energy harvested at UE is set as $M_{\text{EH}} = 3.9$ mW according to [51], while the transmit power is limited within the range between $P_{\min} = 0$ and $P_{max} = 38$ dBm. As a summary, the important simulation parameters are listed in Table 2.

Table 2 Simulation parameters

Parameter	Value
Noise variance at UE j ($\sigma^2_{A_j}$)	− 111 dBm
Noise variance at UE j due to PS ($\sigma^2_{I_j}$)	− 35 dBm
Number of multi-path ($N^p_{i,j}$)	4
Path loss exponent (k)	3
Cell radius for small-cell	20 m
Maximum transmit power (P_{max})	38 dBm
Minimum transmit power ($P_{\min}$)	0
Maximum harvested energy at UE (M^{EH})	3.9 mW [51]
Number of antennas in BS (M_{BS})	3
Number of antennas in UE	1
Circuit specification (a)	1500 [44]
Circuit specification (b)	0.0022 [44]
AC computing requirement (ϵ_{ac})	0.04764 mW [35]
DC energy management requirement (ϵ_{dc})	0.2 mW [35]

8.2 Rate-energy tradeoff

In the first set of experiments, we evaluate the proposed algorithms on the trade-off between the system sum-rate and the energy harvesting with the given energy requirements, in the two network scenarios. To show their names concisely, the quadratic transform-based FP algorithm is denoted by **FP**, the sequential beamforming and power splitting algorithms with ZF, MRT, and SLNR are denoted by **ZF**, **MRT**, and **SLNR**, respectively, which are also the legend names for the small-cell scenario in the following figures. However, to distinguish the applied scenarios, we use **ZF-cf**, **MRT-cf**, and **SLNR-cf**, with the suffix **cf**, as the legend names for the algorithms applied to the cell-free scenario. In addition, we use *'data rate'* and *'system sum-rate'* interchangeably in the following, whenever there is no potential for confusion.

Aided by these legends, it can be seen clearly in Fig. 4a that FP can achieve the highest data rate while trading off the amount of EH in the small-cell scenario. On the other hand, the MRT and SLNR algorithms achieve relatively lower data rates but offer trade-offs similar to FP until they reach their rate limits. In contrast, ZF limits its power towards other UEs, resulting in a reduction in the amount of EH. Moreover, as each ZF BV, $\omega_k, \forall k \in \mathbb{B}_i \backslash i$, is only conducted to transmit towards its own UE k, it could not completely eliminate the interference to a specific UE i with other BVs not defined. As a consequence, the data rate of ZF is also reduced, resulting in the poorest rate-energy trade-off among the algorithms in this scenario.

However, the performance trend of ZF changes in the cell-free scenario, as shown in Fig. 4b. In this scenario, all BSs k will coordinate their transmissions towards a specific UE i, with their other BVs, $\omega_{k,i'}, \forall i' \in \mathbb{U}_k \backslash i$, that would eliminate the interferences towards UE i. Given that, although ZF still suffers from a reduction in EH due to its zero-forcing nature, it can achieve a rate-energy trade-off that is higher than the other algorithms but lower than FP in the high rate region.

Apart from the above, it can be also seen that by controlling the transmit power leaked to other unintended UEs, SLNR could achieve higher data rate than MRT which only scales the transmitted signal to its intended UE. The performance difference in terms of data rate is further amplified in the simulated cell-free scenario where all BSs would coordinate their transmissions to minimize such leakages, resulting in reduced inferences and increased SINRs as expected. Finally, the results for both scenarios are summarized in Fig. 4c, allowing for simultaneous comparison of these algorithms in the different network scenarios.

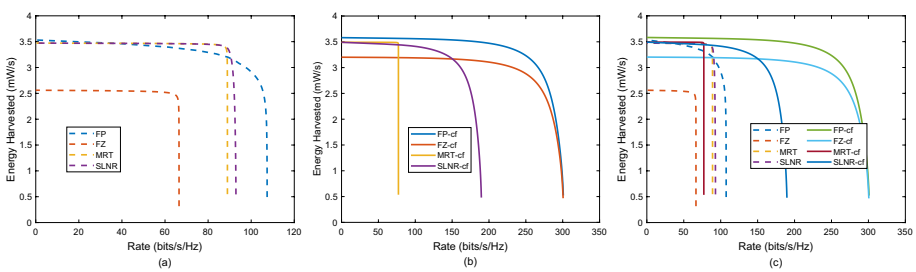

Fig. 4 Rate-energy region: **a** small-cell, **b** cell-free, and **c** all

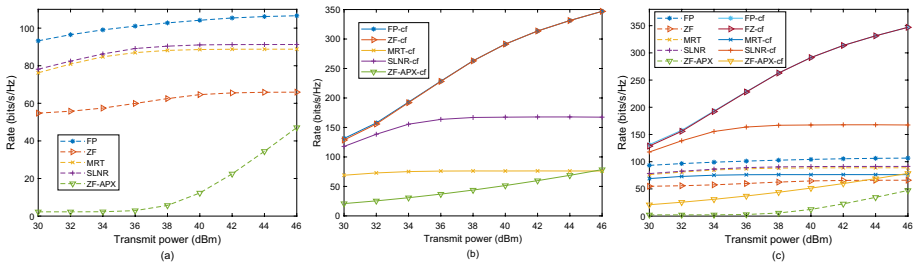

Fig. 5 Data rate with varying transmit power: **a** small-cell, **b** cell-free, and **c** all

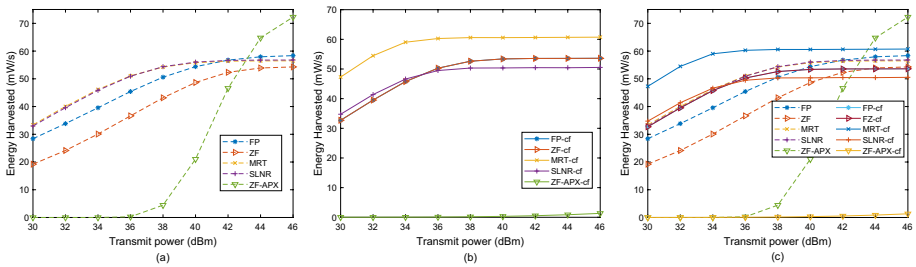

Fig. 6 Energy harvesting with varying transmit power: **a** small-cell, **b** cell-free, and **c** all

8.3 Impact of transmit power

In this set of experiments, we aim to show the impact of the transmit power of BSs on the proposed algorithms in the different scenarios. That is, instead of the trade-off between ID (or data rate) and EH, we consider them individually with respect to the transmit power of BSs. Specifically, by varying the transmit power from 30 to 46 dBm with a step size of 2 dBm, we show the performance of these algorithms on the two metrics (data rate and EH) in Figs 5 and 6, respectively. Here, ZF-APX and ZF-APX-cf denote the baseline algorithm applied to the small cell scenario and the cell-free scenario, respectively, in addition to the others noted before.

Specifically, the performance trend observed in Fig. 5 demonstrates that increasing the transmit power leads to a higher data rate for all the compared algorithms, as expected. On one hand, the data rate performance of ZF, which is the lowest among the algorithms in the small-cell scenario (shown in Fig. 5a), increases and approaches that of FP in the cell-free scenario (shown in Fig. 5b), reflecting the same trend as discussed in the previous subsection. On the other hand, it can be seen in Fig. 5b that, unlike the significant increasing trend observed for both FP and ZF, increasing the transmit power provides only marginal benefits to MRT and SLNR. This confirms the result shown in Ch. 3 of [47] that MRT is good at very low SNR and ZF is good at high SNR when global interference coordination is considered. The above is particularly noteworthy as it also reveals the fact that, without mechanisms to reflect SINR, increasing the transmit power may not effectively improve the data rate, especially for MRT, in the cell-free scenario.

In further numerical terms, the data rates of FP, ZF, MRT, and SLNR in the cell-free scenario are 3.25, 5.26, 0.85, and 1.83 times their values in the small-cell scenario, respectively, when comparing Fig. 5a and b at 46 dBm. This confirms the performance trend reported in [52] that cell-free massive MIMO can provide five-to-tenfold improvement

in throughput over small-cell counterpart. Apart from the expected trend, our results also demonstrate that not all conventional beamforming schemes are suitable for the cell-free scenario, as the numerical examples suggest. Further, our results also show that the amounts of EH obtained by FP, ZF, MRT, and SLNR in the cell-free scenario can be 1.15, 1.70, 1.42, and 1.05 times their values in the small-cell scenario, respectively, at maximum, when comparing Fig. 6a and b at 30 dBm. Clearly, the benefits provided by EH are relatively marginal compared to those for data rate. Despite the difference, these results can compensate for the previous works by showing the distinct trends to be observed in the different scenarios when taking SWIPT into account. In addition, as observed in [29], the rate performance of ZF-APX in the cell-free scenario surpasses that in the small-cell scenario, as expected. However, due to potentially lower path loss in the small-cell scenario, the energy harvested by UE from its AP with ZF-APX using random PSR in the small-cell scenario could exceed that in the cell-free scenario, especially when the transmit power is high. However, maximizing EH is not the objective of this work. In comparison, with a special concern to allocate PSR, our algorithms are able to approach the objective of maximizing the data rate while satisfying the EH requirements, yielding superior performance to the baseline in a majority of the cases in both scenarios.

Finally, through the overall comparisons shown in Figs. 5c and 6c, it could be summarized that augmenting the transmit power leads to a substantial enhancement in the data rate of both FP and ZF, transitioning from the small-cell to the cell-free scenario, as exhibited in Fig. 5c. However, for the other algorithms, increasing the transmit power may not have a substantial impact during the same transition, as evident from the performance metrics (data rate and EH) shown in Figs. 5c and 6c.

8.4 Impact of number of cells

In this set of experiments, we vary $N_b \in \{6, 9, 12, 15, 19\}$ while setting the transmit power to 38 dBm and keeping the other parameters fixed to investigate the impacts of these algorithms on the network size in the different network scenarios. It is also assumed that $\mathbb{B}_i = \mathbb{B}, \forall i$, and $\mathbb{U}_i = \mathbb{U}, \forall i$, as the previous, regardless of the network size. In addition, given a network size composed of N_b cells, the cell-free scenario is similarly obtained by placing the BSs at the same positions as in the small-cell scenario, which eliminates the cell boundaries and results in a similar network setup.

Now, by taking a broader perspective on examining and comparing the results shown in Figs. 7 and 8, we can see that increasing the number of cells, or network size, has a more pronounced impact on the performance on EH than on the data rate. This could reflect the fact that the performance on EH is more related to the total received power in (4) which could more proportionally increase as the network size increases, as shown in Fig. 8. In contrast, the performance on data rate is related to SINR in (5) in the cell-free scenario or (34) in the small-cell scenario. In either one, SINR is a ratio between the desired power and the sum of interference power and noise, and its numerator and enumerator could increase with varying degrees as the network size increases, depending on the different algorithms applied. Thus, the increased network size is not necessary to proportionally increase the data rate, as shown in Fig. 7.

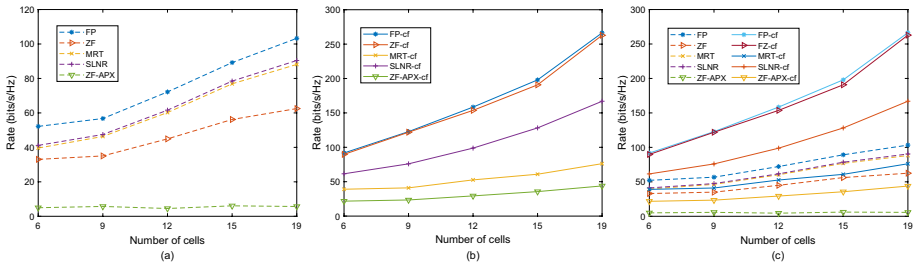

Fig. 7 Data rate with varying number of cells: **a** small-cell, **b** cell-free, and **c** all

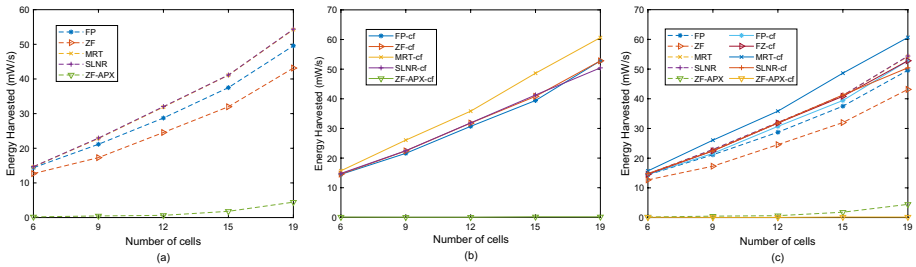

Fig. 8 Energy harvesting with varying number of cells: **a** small-cell, **b** cell-free, and **c** all

Next, by taking a closer look to compare these results, we can see that while the relative performance of each algorithm remains consistent within each network scenario, there are discernible performance trends across the two metrics as the network size increases. For example, when compared with itself in the small-cell scenario, MRT becomes the worst to provide the data rate in the cell-free scenario, with very limited enhancements by increasing the network size. This result aligns with the findings shown previously and is further confirmed here by varying the network size. Similarly, the other algorithms also exhibit a trend of increasing the data rate as the network size increases, but yield more improvements with the same increase in the size. Moreover, with the middle of the transmit power range, i.e. 38 dBm, the proposed algorithms consistently outperform the baseline algorithm, ZF-APX, in terms of both data rate and energy harvesting, regardless of the network size.

According to the above including those in the previous sets of experiments, we could conclude that the sequential beamforming and power splitting algorithms would be significantly influenced by the adopted beamforming schemes while reducing the computational complexity. In this context, ZF is a good option that provides a reasonable trade-off in the cell-free scenario, and especially it can approach the near-optimal data rate realized by FP in this scenario. In contrast, MRT and SLNR can serve as good strategies in the small-cell scenario, offering a high rate-energy trade-off similar to FP until reaching their maximum data rates. Among them, SLNR would be a more versatile strategy as it combines the respective benefits of MRT and ZF, as noted in [47]. However, if feasible, FP is the preferred choice for near-optimal solutions, even if it may take more time to iteratively approach the optimum.

9 Conclusion

In this work, we have focused on addressing joint optimization problems related to downlink (DL) beamforming vectors (BVs) and power splitting ratios (PSRs) in simultaneous wireless information and power transfer (SWIPT)-enabled cell-free massive multiple-input multiple-output (MIMO) networks and small-cell networks. Our objective has been made to maximize the sum-rate while considering the constraints on harvested energy, AC logic energy supply, and total transmit power in these networks. To tackle the non-convex nature of these optimization problems, we have proposed quadratic transform-based fractional programming (FP) algorithms that can iteratively provide near-optimal solutions. To further reduce the time complexity, we have also applied conventional schemes such as zero forcing (ZF), maximum ratio transmission (MRT), and signal-to-leakage-and-noise ratio (SLNR) for beamforming vector (BV) design, while incorporating the one-dimensional search algorithm for power splitting ratio (PSR) design within the FP-based framework.

Through simulation studies, we have examined the performance differences among these algorithms in terms of system sum-rate, energy harvesting (EH), and rate-energy region as the trade-off between the two metrics. More specifically, we have shown that under the condition of this work that data rate is the objective while energy harvesting is considered as constraint, the proposed algorithms enable cell-free massive MIMO to achieve data rates up to nearly five times higher than small-cell MIMO, with limited energy harvested through SWIPT. They also outperform the baseline in both scenarios in general. Among them, FP emerges as the preferred option for near-optimal solutions, while the remaining algorithms offer versatility for diverse situations.

As a conclusion, our findings shed light on the aspects that have not been extensively explored in previous works. However, due to space constraints, there are still further research directions that warrant investigation. For instance, exploring algorithms for long-term optimization, based on the FP algorithms and their variants in the different network scenarios, would be an interesting avenue for future research.

Abbreviations

SWIPT	Simultaneous wireless information and power transfer
MIMO	Multiple-input multiple-output
MISO	Multiple-input single-output
BS	Base station
UE	User equipment
AC	Alternating current
DC	Direct current
FP	Fractional programming
ID	Information decoding
EH	Energy harvesting
ZF	Zero forcing
MRT	Maximum ratio transmission
SINR	Signal-to-interference-and-noise ratio
SLNR	Signal-to-leakage-and-noise ratio
BV	Beamforming vector
CV	Channel vector
PS	Power splitting
PSR	Power splitting ratio
UL	Uplink
DL	Downlink
CPU	Central processing unit
QoS	Quality of service
CoMP	Coordinated multi-point transmission
IoT	Internet of thing

WPT	Wireless power transfer
EE	Energy efficiency
FPP–SCA	Feasible point pursuit–successive convex approximation
MM	Majorization–minimization
BD	Block diagonalization
MMSE	Minimum mean square error
RF	Radio frequency

Author contributions
All authors contribute to the concept, the design, and developments of the algorithm and the simulation results in this manuscript. All authors read and approved the final manuscript.

Funding
This work was supported by the National Science and Technology Council, Republic of China, under grant 111-2221-E-126-003.

Availability of data and materials
Not applicable.

Code availability
Not applicable.

Declarations

Ethics approval and consent to participate
Not applicable.

Consent for publication
Not applicable.

Competing interests
The authors declare that they have no competing interests.

Received: 8 September 2023 Accepted: 2 April 2024
Published online: 17 April 2024

References

1. M.K. Karakayali, G.J. Foschini, R.A. Valenzuela, Network coordination for spectrally efficient communications in cellular systems. IEEE Wirel. Commun. **13**(4), 56–61 (2006). https://doi.org/10.1109/MWC.2006.1678166
2. S. Mukherjee, D. Kim, J. Lee, Base station coordination scheme for multi-tier ultra-dense networks. IEEE Trans. Wireless Commun. **20**(11), 7317–7332 (2021). https://doi.org/10.1109/TWC.2021.3082625
3. A. Lozano, R.W. Heath, J.G. Andrews, Fundamental limits of cooperation. IEEE Trans. Inf. Theory **59**(9), 5213–5226 (2013). https://doi.org/10.1109/TIT.2013.2266995
4. G. Interdonato, E. Björnson, H. Quoc-Ngo et al., Ubiquitous cell-free massive MIMO communications. J. Wirel. Commun. Netw. (2019). https://doi.org/10.1186/s13638-019-1507-0
5. H.I. Obakhena, A.L. Imoize, F.I. Anyasi et al., Application of cell-free massive MIMO in 5G and beyond 5G wireless networks: a survey. J. Eng. Appl. Sci. **68**, 13 (2021). https://doi.org/10.1186/s44147-021-00131-x
6. Y. Hou, L. Zitoune, V. Vèque, Fluid-based energy efficiency analysis of JT-CoMP scheme in Femto cellular networks. IEEE Trans. Green Commun. Netw. **5**(1), 133–145 (2021). https://doi.org/10.1109/TGCN.2020.3036903
7. L.-H. Shen, C.-Y. Su, K.-T. Feng, CoMP enhanced subcarrier and power allocation for multi-numerology based 5G-NR networks. IEEE Trans. Veh. Technol. **71**(5), 5460–5476 (2022). https://doi.org/10.1109/TVT.2022.3154896
8. R. Singh, D. Saluja, S. Kumar, Graph Based Training Resource Allocation Scheme for CoMP Transmission in CRAN: A Low Complexity Solution. IEEE Trans. Netw. Sci. Eng. **8**(3), 2402–2411 (2021). https://doi.org/10.1109/TNSE.2021.3093311
9. M.M. Abdelhakam, M.M. Elmesalawy, I.I. Ibrahim et al., Joint trajectory and CoMP clustering optimization in UAV-assisted cellular systems: a coalition formation game approach. J. Wirel. Commun. Netw. (2023). https://doi.org/10.1186/s13638-023-02302-y
10. M.S.J. Solaija, H. Salman, A.B. Kihero, M.I. Sağlam, H. Arslan, Generalized coordinated multipoint framework for 5G and beyond. IEEE Access **9**, 72499–72515 (2021). https://doi.org/10.1109/ACCESS.2021.3079190
11. J. Khan, L. Jacob, Resource allocation for CoMP enabled URLLC in 5G C-RAN architecture. IEEE Syst. J. **15**(4), 4864–4875 (2021). https://doi.org/10.1109/JSYST.2020.3018308
12. J. Sultan, W.A. Jabbar, N.S. Al-Thobhani, A. Al-Hetar, Downlink performance of coordinated multipoint (CoMP) in next generation heterogeneous networks, in *2023 3rd International Conference on Emerging Smart Technologies and Applications (eSmarTA)* (2023), pp. 1–8. https://doi.org/10.1109/eSmarTA59349.2023.10293486
13. G. Interdonato, E. Björnson, H. Quoc Ngo, E.G. Larsson, Ubiquitous cell-free massive MIMO communications. EURASIP J. Wirel. Commun. Netw. **2019**, 197 (2019). https://doi.org/10.1186/s13638-019-1507-0
14. H.Q. Ngo, A. Ashikhmin, H. Yang, E.G. Larsson, T.L. Marzetta, Cell-free massive MIMO versus small cells. IEEE Trans. Wirel. Commun. **16**(3), 1834–1850 (2017). https://doi.org/10.1109/TWC.2016.2647076

15. D. Van Leemput, A. Sabovic, K. Hammoud, J. Famaey, S. Pollin, E. De Poorter, Energy harvesting for wireless IoT use cases: a generic feasibility model and tradeoff study. IEEE Internet Things J. **10**(17), 15025–15043 (2023). https://doi.org/10.1109/JIOT.2023.3263543
16. C. Delgado, J.M. Sanz, C. Blondia, J. Famaey, Batteryless LoRaWAN communications using energy harvesting: modeling and characterization. IEEE Internet Things J. **8**(4), 2694–2711 (2021). https://doi.org/10.1109/JIOT.2020.3019140
17. Z. Wei, X. Yu, D.W.K. Ng, R. Schober, Resource allocation for simultaneous wireless information and power transfer systems: a tutorial overview. Proc. IEEE **110**(1), 127–149 (2021)
18. D. Masotti, M. Shanawani, G. Murtaza, G. Paolini, A. Costanzo, RF systems design for simultaneous wireless information and power transfer (SWIPT) in automation and transportation. IEEE J. Microw. **1**(1), 164–175 (2021)
19. G. Dong, H. Zhang, D. Yuan, Downlink achievable rate of massive MIMO enabled SWIPT systems over Rician channels. IEEE Commun. Lett. **22**(3), 578–581 (2018). https://doi.org/10.1109/LCOMM.2018.2792419
20. X. Chen, X. Wang, X. Chen, Energy-efficient optimization for wireless information and power transfer in large-scale MIMO systems employing energy beamforming. IEEE Wirel. Commun. Lett. **2**(6), 667–670 (2013). https://doi.org/10.1109/LWC.2013.100313.130484
21. H.T. Demir, T.E. Tuncer, Antenna selection and hybrid beamforming for simultaneous wireless information and power transfer in multi-group multicasting systems. IEEE Trans. Wireless Commun. **15**(10), 6948–6962 (2016). https://doi.org/10.1109/TWC.2016.2594074
22. J. Rubio, A. Pascual-Iserte, D.P. Palomar, A. Goldsmith, Joint optimization of power and data transfer in multiuser MIMO systems. IEEE Trans. Signal Process. **65**(1), 212–227 (2017). https://doi.org/10.1109/TSP.2016.2614794
23. G. Yang, C. Ho, R. Zhang, Y. Guan, Throughput optimization for massive MIMO systems powered by wireless energy transfer. IEEE J. Sel. Areas Commun. **33**(8), 1640–1650 (2015). https://doi.org/10.1109/JSAC.2015.2434120
24. L. Zhao, X. Wang, K. Zheng, Downlink hybrid information and energy transfer with massive MIMO. IEEE Trans. Wirel. Commun. **15**(2), 1309–1322 (2016). https://doi.org/10.1109/TWC.2015.2472203
25. T.C. Mai, H.Q. Ngo, M. Egan, T.Q. Duong, Pilot power control for cell-free massive MIMO. IEEE Trans. Veh. Technol. **67**(11), 11264–11268 (2018). https://doi.org/10.1109/TVT.2018.2878793
26. T.X. Doan, H.Q. Ngo, T.Q. Duong, K. Tourki, On the performance of multigroup multicast cell-free massive MIMO. IEEE Commun. Lett. **21**(12), 2642–2645 (2017). https://doi.org/10.1109/LCOMM.2017.2764706
27. E. Bjornson, L. Sanguinetti, Making cell-free massive MIMO competitive with MMSE processing and centralized implementation. IEEE Trans. Wirel. Commun. **19**(1), 77–90 (2020). https://doi.org/10.1109/TWC.2019.2940875
28. M. Elwekeil, A. Zappone, S. Buzzi, Optimal joint beamforming and power control in cell-free massive MIMO downlink, in *2021 IEEE 22nd International Workshop on Signal Processing Advances in Wireless Communications (SPAWC)* (2021), pp. 81–85. https://doi.org/10.1109/SPAWC51858.2021.9593141
29. E. Nayebi, A. Ashikhmin, T.L. Marzetta, H. Yang, B.D. Rao, Precoding and power optimization in cell-free massive MIMO systems. IEEE Trans. Wirel. Commun. **16**(7), 4445–4459 (2017). https://doi.org/10.1109/TWC.2017.2698449
30. Ö.T. Demir, E. Björnson, Max–min fair wireless-powered cell-free massive MIMO for uncorrelated rician fading channels, in *2020 IEEE Wireless Communications and Networking Conference (WCNC)* (2020), pp. 1–6. https://doi.org/10.1109/WCNC45663.2020.9120654
31. Ö.T. Demir, E. Björnson, Joint power control and LSFD for wireless-powered cell-free massive MIMO. IEEE Trans. Wirel. Commun. **20**(3), 1756–1769 (2021). https://doi.org/10.1109/TWC.2020.3036281
32. X. Wang, A. Ashikhmin, X. Wang, Wirelessly powered cell-free IoT: analysis and optimization. IEEE Internet Things J. **7**(9), 8384–8396 (2020). https://doi.org/10.1109/JIOT.2020.2990378
33. X. Wang, X. Wang, A. Ashikhmin, Long-term scheduling and power control for wirelessly powered cell-free IoT. IEEE Internet Things J. **8**(1), 332–344 (2021). https://doi.org/10.1109/JIOT.2020.3003646
34. S. Kusaladharma, W.-P. Zhu, W. Ajib, G. Amarasuriya, Performance of SWIPT in cell-free massive MIMO: a stochastic geometry based perspective, in *Proceedings IEEE 17th Annual Consumer Communications & Networking Conference (CCNC)* (2020), pp. 1–6. https://doi.org/10.1109/CCNC46108.2020.9045291
35. H.-V. Tran, G. Kaddoum, Robust design of AC computing-enabled receiver architecture for SWIPT networks. IEEE Wirel. Commun. Lett. **8**(3), 801–804 (2019). https://doi.org/10.1109/LWC.2019.2894118
36. B. Kianbakht, N. Reisi, M. Akbari, Distributed and centralized subcarrier-based precoding for cell-free massive MIMO networks. in *2020 28th Iranian Conference on Electrical Engineering (ICEE)* (2020), pp. 1–5. https://doi.org/10.1109/ICEE50131.2020.9261021
37. X. Xu, M. Tao, Modeling, analysis, and optimization of caching in multi-antenna small-cell networks. IEEE Trans. Wirel. Commun. **18**(11), 5454–5469 (2019). https://doi.org/10.1109/TWC.2019.2936390
38. A. Alkhateeb, O. El Ayach, G. Leus, R.W. Heath, Channel estimation and hybrid precoding for millimeter wave cellular systems. IEEE J. Sel. Top. Signal Process. **8**(5), 831–846 (2014). https://doi.org/10.1109/JSTSP.2014.2334278
39. R.W. Heath, N. Gonzáilez-Prelcic, S. Rangan, W. Roh, A.M. Sayeed, An overview of signal processing techniques for millimeter wave MIMO systems. IEEE J. Sel. Top. Signal Process. **10**(3), 436–453 (2016). https://doi.org/10.1109/JSTSP.2016.2523924
40. P. Schniter, A. Sayeed, Channel estimation and precoder design for millimeter-wave communications: the sparse way, in *2014 48th Asilomar Conference on Signals, Systems and Computers* (2014), pp. 273–277. https://doi.org/10.1109/ACSSC.2014.7094443
41. S. Dahiya, A.K. Singh, Channel estimation and channel tracking for correlated block-fading channels in massive MIMO systems. Digital Commun. Netw. **4**(2), 138–147 (2018). https://doi.org/10.1016/j.dcan.2017.07.006
42. Y. Lin, S. Jin, M. Matthaiou, X. You, Transceiver design with UCD-based hybrid beamforming for millimeter wave massive MIMO. IEEE Trans. Commun. **67**(6), 4047–4061 (2019). https://doi.org/10.1109/TCOMM.2019.2901690
43. J. Xu, R. Zhang, Throughput optimal policies for energy harvesting wireless transmitters with non-ideal circuit power. IEEE J. Sel. Areas Commun. **32**(2), 322–332 (2014). https://doi.org/10.1109/JSAC.2014.141212
44. K. Xiong, B. Wang, K.J.R. Liu, Rate-energy region of SWIPT for MIMO broadcasting under nonlinear energy harvesting model. IEEE Trans. Wirel. Commun. **16**(8), 5147–5161 (2017). https://doi.org/10.1109/TWC.2017.2706277
45. K. Shen, W. Yu, Fractional programming for communication systems-Part I: power control and beamforming. IEEE Trans. Signal Process. **66**(10), 2616–2630 (2018). https://doi.org/10.1109/TSP.2018.2812733

46. W. Dinkelbach, On nonlinear fractional programming. Manag. Sci. **13**(7), 492–498 (1967)
47. E. Björnson, E. Jorswieck et al., Optimal resource allocation in coordinated multi-cell systems. Found. Trends® Commun. Inf. Theory **9**(2–3), 113–381 (2013)
48. J. Ge, Y.-C. Liang, J. Joung, S. Sun, Deep reinforcement learning for distributed dynamic MISO downlink-beamforming coordination. IEEE Trans. Commun. **68**(10), 6070–6085 (2020)
49. Python Software Foundation: Python 3.7.13 (2022). https://www.python.org/downloads/release/python-3713/
50. MathWorks: MATLAB 2019b (2019). https://www.mathworks.com/products/matlab.html
51. P.V. Tuan, I. Koo, Optimizing efficient energy transmission on a SWIPT interference channel under linear/nonlinear EH models. IEEE Syst. J. **14**(1), 457–468 (2020). https://doi.org/10.1109/JSYST.2019.2924265
52. H.Q. Ngo, A. Ashikhmin, H. Yang, E.G. Larsson, T.L. Marzetta, Cell-free massive MIMO versus small cells. IEEE Trans. Wirel. Commun. **16**(3), 1834–1850 (2017). https://doi.org/10.1109/TWC.2017.2655515

Publisher's Note